From the Department of Diagnostic and Interventional Radiology
University Hospital of Würzburg

Director: Professor Dr. med. Thorsten Bley

Comparison between Dual-Energy-CT perfusion imaging and perfusion-weighted SElf-gated Non-Contrast-Enhanced FUnctional MR imaging of the lung in patients with pulmonary artery embolism

Inaugural dissertation

To obtain a doctoral degree from the Medical Faculty of the

Julius-Maximilians-University Würzburg

presented by

Cristina Maria Klinnert Vlachopoulou

from Madrid, Spain

Würzburg, October 2022

Speaker: Prof. Dr. med. Simon Veldhoen, MHBA

Co-speaker: Prof. Dr. med. Matthias Eyrich

Dean: Prof. Dr. med. Matthias Frosch

Date of oral exam: **21.4.23**

The doctoral student is a physician.

Table of contents

1 Introduction..... 1
2 Background..... 3
2.1 The lung..... 3
2.1.1 Anatomy and function of the lung..... 3
2.1.2 Airway..... 5
2.1.3 Pulmonary vascular anatomy..... 6
2.1.4 Pulmonary embolism..... 8
2.2 CTPA and DECT..... 13
2.3 MRI..... 17
2.4 SENCEFUL MRI..... 22
3 Material and methods..... 24
3.1 Study design..... 24
3.2 Study population..... 24
3.3 Study tools..... 25
3.4 Data analysis..... 25
4 Results..... 30
4.1 CTPA..... 30
4.2 Iodine color-coded maps of DECT..... 30
4.3 SENCEFUL MRI..... 31
4.4 SENCEFUL MRI and iodine color-coded maps of DECT..... 33
5 Discussion..... 35
6 Study limitations..... 44
7 Summary..... 47
8 Zusammenfassung..... 49
9 References..... 51

10 Appendix

I List of abbreviations

II List of figures

III List of tables

IV Acknowledgments

1. Introduction

Pulmonary artery embolism (PE) is a common condition (annual incidence rate of 39–115 per 100 000 population, depending on the country (1)), and an even more common clinical suspect. The computed tomography pulmonary angiogram (CTPA) is the main medical imaging tool used to diagnose a suspected case of PE (2). With the CTPA, a thrombus can be identified by the lack of filling of a pulmonary artery or a branch thereof with a contrast agent following its intravenous application. CTPA yields a sensitivity of 83 % and a specificity of 96 % for the diagnosis of PE (3). However, no conclusions about the perfusion, or rather the perfusion impairment in the case of PE, can be drawn from the images of standard CTPA, which are acquired at a single time point. Another main disadvantage when performing computed tomography (CT) is the radiation exposure which limits its use in multiple sessions and risk groups such as young patients or pregnant women. In the monitoring of chronic pulmonary diseases and their complications, which commonly need repeated imaging, the radiation exposure of CT can be an important issue (4). The risks of radiation exposure are mainly divided into stochastic and deterministic effects. The stochastic effects refer to the random genetic effects of radiation exposure including cancer induction whereas the deterministic effects refer to the damage of a given tissue depending on specific radiation doses, e.g. transient erythema at 2 gray (Gy) or permanent epilation at 7 Gy (4). The effective dose of a chest CT with contrast is in a range of 4.9-12 millisieverts (mSv) (5), whereas that of chest radiography in two views is in a range of 0.06–0.25 mSv (6). In a study by Petritsch et al. (7), the application of Dual-Energy CT (DECT), which was also applied in this work, was found to have a lower effective dose compared to conventional CTPA.

The clinical presentation of PE can vary significantly as it can be accompanied by dyspnea, hypoxemia, or chest pain or can even be asymptomatic. Thus, it is important to know which individual functional consequence a certain PE has. To gain a better impression of the effects of a PE on the perfusion and hence the gas exchange, a functional imaging method is beneficial. One approach for functional imaging using radiation exposure is the generation

of color-coded iodine perfusion maps acquired by DECT, which enable the detection of perfusion defects in the pulmonary parenchyma (8).

Today, magnetic resonance imaging (MRI), has overtaken the use of CT in some diagnostic fields, such as neuroimaging. MRI is a non-invasive imaging tool without radiation exposure, which uses a magnetic field and radio frequency waves to interact with the protons in the body, which thereby emit energy that is captured by the scanner and is the basis to produce the resultant image. When the lung and its pathologies need to be examined, MRI has many obstacles, mainly because of the low parenchymal density of protons, the magnetic field inhomogeneities in the lung, and constant tissue movement due to respiration. In contrast to the existing approach of DECT with iodine color-coded maps, the SElf-gated Non-Contrast-Enhanced FUnctional Lung (SENCEFUL) MRI technique offers the possibility to interpret perfusion maps without any radiation exposure or application of contrast agents (9,10). The measurement in SENCEFUL MRI can be performed during conditions of free breathing and without electrocardiogram (ECG) triggering.

The purpose of this study was to determine whether PE can be diagnosed on the basis of visible perfusion defects in the perfusion maps of SENCEFUL MRI and in the iodine-coded maps of DECT and to compare the diagnostic performance of these methods. Both SENCEFUL-MRI and iodine distribution maps from DECT have been compared with the gold standard for the diagnosis of pulmonary embolism, namely CTPA. Additionally, the functional images were compared with each other on a per-patient basis.

2. Background

2.1 The lung

2.1.1 Anatomy and function of the lung

The lungs are the organs that are responsible for the gas exchange in an organism and comprise a right and a left lung which are located in the thoracic cavity. Each lung is divided into lobes. The right lung is separated into three lobes (superior, middle, and inferior lobe). The oblique fissure divides the lung into the inferior lobe and middle/superior lobe and the horizontal fissure separates the middle and superior lobe (11). The left lung is divided into two lobes (superior and inferior lobe) by the oblique fissure (11) (Figure 1).

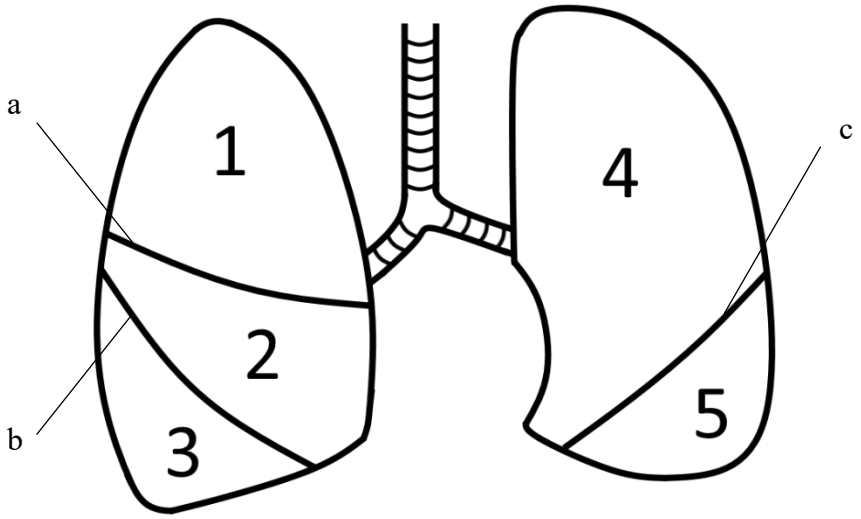

Figure 1: The lung: 1 – superior right lobe; 2 – middle right lobe; 3 – inferior right lobe; 4 – superior left lobe; 5 – inferior left lobe; a – horizontal fissure right; b – oblique fissure right; c – oblique fissure left.

The three right lobes are subdivided into 10 segments. The superior lobe is divided into three segments (apical, posterior, and anterior), the middle lobe into two (medial and lateral), and the inferior into five (apical, anterior, medial, posterior, and lateral). The two left lobes are divided into eight to nine segments. The superior lobe has four segments (anterior,

apicoposterior, and two corresponding to the lingula: inferior and superior). The inferior lobe has four or five segments (lateral, anteromedial, superior, posterior) (12).

The lung is surrounded by the pleura. The visceral pleura covers the lung surface including the fissures, and the parietal pleura is in contact with the thoracic wall. In this pleural cavity, negative intrapleural pressure ensures that the lungs can expand during inspiration and do not collapse during expiration. There is a small amount of serous fluid in the cavity, which permits the displacement of the visceral pleura against the parietal pleura. The act of breathing itself occurs with the aid of the diaphragm and the intercostal muscles.

The gas exchange takes place in the alveoli. Deoxygenated blood is transported in the pulmonary arteries, which originate in the right ventricle of the heart and end up in the alveolar-capillary beds. In these capillaries, carbon dioxide is emitted in exchange for oxygen. The oxygenated blood is transported through the veins and enters the left atrium through four pulmonary veins.
The alveolar epithelium consists of five cell types: type I pneumocytes (90–95 % of the alveolar epithelium), type II pneumocytes, brush cells, club cells, and alveolar macrophages (13). The blood-gas barrier is the term for the tissue between the air in the alveoli and the blood in the capillaries. The components of this barrier are the alveolar cells, the basal laminae, and the endothelial cells of the capillaries (13).

The ventilation and the perfusion of the lungs are necessary for adequate gas exchange. The perfusion refers to the blood flow within the capillaries and the ventilation to the airflow to the alveoli.

2.1.2 Airway

The respiratory system is divided into the upper and lower respiratory tract. The upper respiratory system consists of the nasal cavities and sinuses, as well as the pharynx, tonsils, and larynx. The lower airways consist of the trachea and the bronchial tree (14). The trachea is divided into the right and left primary bronchi, which then divide into lobar and subsequently segmental bronchi. The division into the primary bronchi is located at vertebra T5 (15) whereas the origin of the right primary bronchus is higher. The bronchi enter the lung through the hilum, where the arteries, veins, and lymphatics join. The trachea and the bronchi are constructed from cartilaginous walls. The segmental bronchi end in terminal bronchioles, which subsequently terminate in a respiratory bronchiole. In contrast to the bronchi, the terminal bronchioles do not have a cartilaginous wall (15). The respiratory bronchiole transports inhaled air to the alveolar ducts, which subsequently divide into alveolar sacs that end in the alveoli (Figure 2). There are more than 300 million alveoli in an adult (16).

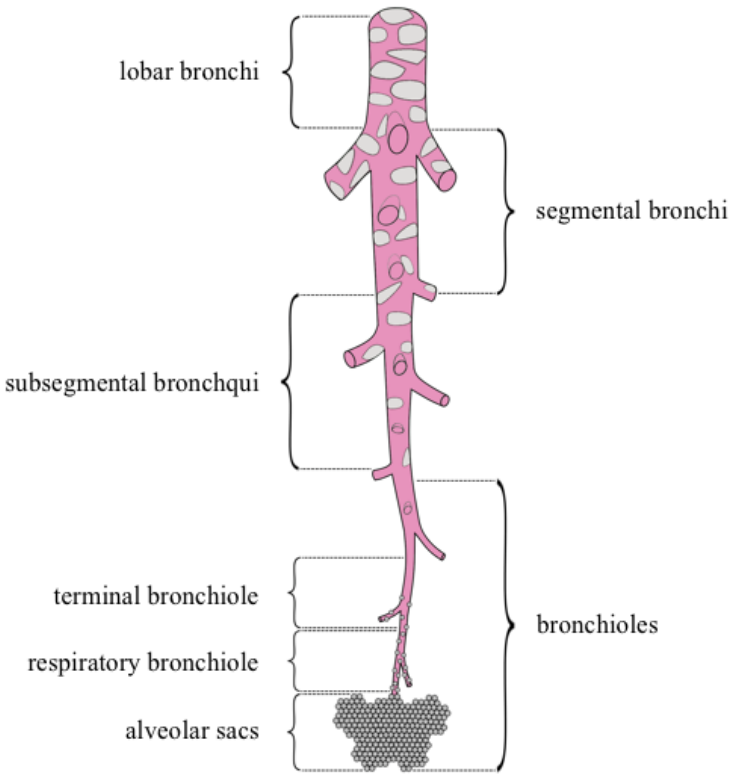

Figure 2: A schematic representation of the bronchial tree, following reference (17).

2.1.3 Pulmonary vascular anatomy

The blood circulation of the lung consists of the pulmonary arteries, the pulmonary veins, and the bronchial vessels. PE occurs in the pulmonary arteries.

The pulmonary arteries are divided into the lobar, segmental, and sub-segmental parts and are named according to the bronchopulmonary segment of the lung they supply. The origin of the main pulmonary artery is the right ventricle, it is divided into the right and left pulmonary artery. The anatomical correlation for this bifurcation is the carina.

The right pulmonary artery, which supplies blood to the three right lobes, bifurcates into the right truncus anterior and the interlobar pulmonary artery. The right truncus anterior is responsible for the blood supply of the superior lobe and the interlobar pulmonary artery for the middle and inferior lobe (18). There are three segmental arteries for the superior lobe for each bronchopulmonary segment, namely the anterior, apical, and posterior segment artery. It should be noted that there can be interindividual differences regarding the branches' origins. The interlobar artery provides the medial and lateral segment of the middle lobe by either one common branch, which separates later, or by two branches, respectively. After the origin of the medial and lateral arteries, the interlobar artery also yields branches for the lower lobe, one superior segment artery, and one anterior, medial, lateral, and posterior basal segment artery (18).

The left pulmonary artery has to supply blood to two lobes: the superior lobe with its four segments (anterior, apicoposterior, and two corresponding to the lingula: inferior and superior) and the inferior lobe with its four to five segments (lateral, anteromedial, superior, posterior) (12). Each segment is supplied by a segmental artery named by the segment itself.

The pulmonary arteries end up in pulmonary capillaries, which surround the alveoli. The capillaries then connect to the pulmonary veins, which are responsible for the transport of the oxygenated blood to the left atrium, as described before.

The bronchial arteries supply blood to the intrathoracic components, such as the lung (trachea, bronchial tree, pleura) and part of the esophagus. There are several interindividual variations in the anatomy of the bronchial arteries. In the majority, the bronchial arteries consist of two left ones, originating from the anterior wall of the descending aorta and one right bronchial artery, arising most commonly from an intercostal artery of the posteromedial part of the aorta. In the distal parts they anastomose with the pulmonary arteries (19). The venous drainage takes place mainly through the pulmonary veins.

2.1.4 Pulmonary embolism

A PE is a venous thromboembolism. A blood clot, which has been formed in a systemic vein previous to the right side of the heart or in the right heart itself, obstructs one or more arteries in the lung and subsequently leads to a deficiency of blood supply to the downstream lung parenchyma. In most cases, the origin is a deep venous thrombosis of a lower limb. If severe, the PE can lead to a failure of the right ventricle caused by an increased pulmonary vascular resistance, which subsequently can lead to death. The annual incidence of PE ranges from 39 to 115/100 000 population (1). In Germany, the annual incidence measured in 2015 was 109/100 000 (20).

In general, a PE has a non-specific clinical presentation. It can be asymptomatic, but can also be associated with dyspnea (with or without hypoxemia), chest pain, syncope, or other symptoms (21). However, none of the mentioned symptoms are ubiquitous and the chest pain can be similar to that experienced in cases of angina pectoris. If the location of the PE is central, the differential diagnoses are acute coronary syndrome and aortic dissection. Tachycardia (38 % of patients), T-wave inversion in V1 (38 % of patients), and ST elevation in aVR (36 % of patients) are the most common ECG changes observed in patients with PE (22). A heart rate of over 100/min, an S1Q3T3 pattern, a complete right bundle branch block, an inverted T-wave in V1–V4, and an ST elevation or atrial fibrillation, are six signs in ECG that have a prognostic value and can be related to a higher risk of death and circulatory shock (22). While hemodynamic instability can be present in patients with an extended PE, it is not frequent (2). Since the non-specific clinical presentation makes diagnosis challenging, an algorithm facilitates the diagnosis of a PE.

According to the 2019 European Society of Cardiology (ESC) Guidelines for the diagnosis management of acute PE, a clinical probability (pre-test) should first be defined by using prediction rules, such as the Geneva (23) or Wells rules (24) (Tables 1 and 2).

The revised Geneva score	
age >65 years	1
previous DVT/PE	3
surgery/fracture within 1 month	2
active malignant condition	2
unilateral lower-limb pain	3
hemoptysis	2
heart rate 75–94/min	3
heart rate >94/min	5
pain on lower-limb deep venous palpation and unilateral edema	4
clinical probability	
low	0–3
intermediate	4–0
high	>10
PE unlikely	0–5
PE likely	>5

Table 1: Revised Geneva score.

Wells score	
clinical signs of DVT	3
alternative diagnosis less likely than PE	3
heart rate >100/min	1.5
immobilization/surgery in the previous weeks	1.5
previous DVT/PE	1.5
hemoptysis	1
malignancy	1
clinical probability	
low	<2
intermediate	2–6
high	>6
PE unlikely	0–4
PE likely	>4

Table 2: Wells score.

PE: pulmonary embolism, DVT: deep vein thrombosis.

In hemodynamically stable patients, D-dimer testing should follow after assigning a low or intermediate clinical probability. If the D-dimers are negative, no treatment is indicated. If the D-dimer test is positive, a CTPA should be performed, according to the guidelines. However, CTPA should directly be considered to confirm the diagnosis if a high clinical probability of PE/PE likely was defined or when a hemodynamically unstable patient shows a right ventricular dysfunction in the transthoracic echocardiogram (2).

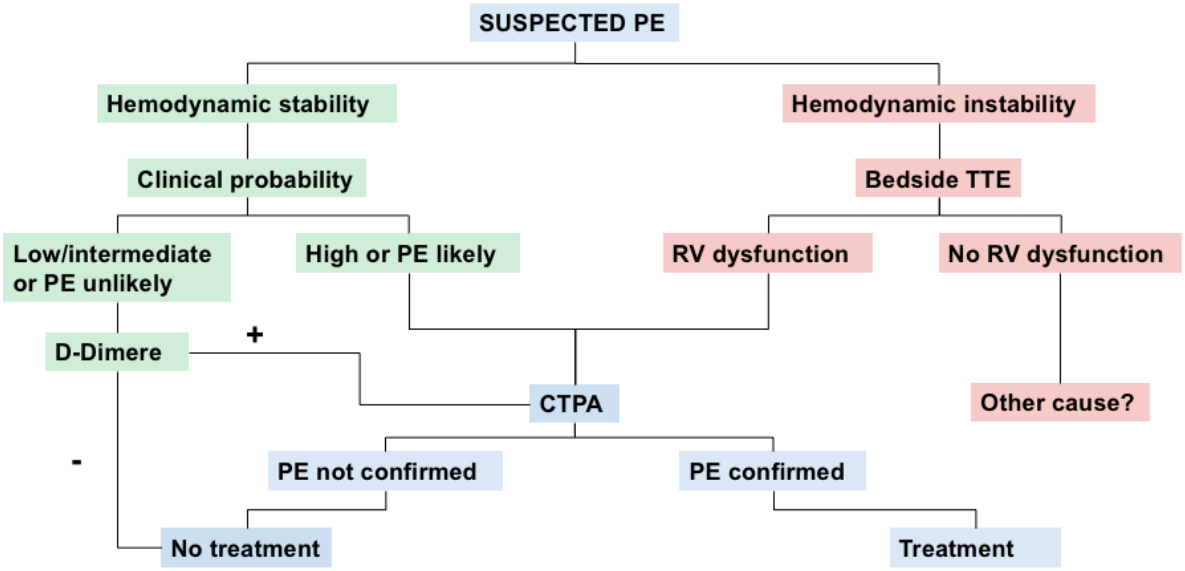

Figure 3: Diagnostic algorithm of PE. PE: pulmonary embolism; TTE: transthoracic echocardiogram; RV dysfunction: right ventricular dysfunction; CTPA: computed tomography pulmonary angiogram, following reference (2).

The CTPA is the gold standard of the currently available imaging tools used to diagnose a PE. In the Prospective Investigation of Pulmonary Embolism II (PIOPIED II) study, it was concluded that the CTPA has a sensitivity of 83 % and a specificity of 96 % (3). As a reference standard for the diagnosis of a PE, a ventilation-perfusion lung scan, pulmonary digital-subtraction angiography, or venous ultrasonography was used. The positive predictive value was 86 % and the negative predictive value was 95 %. The study described how important the pre-test probability is, e.g., in cases with a low clinical probability for PE, the CTPA yielded a rather low positive predictive value (58 %), but a high negative predictive value (96 %). On the contrary, in the case of a high clinical probability, the positive predictive value was high (96 %) and the negative predictive value was rather low (60 %) (3).

In summary, when the CTPA is normal in patients with a low or intermediate clinical probability/PE unlikely, it excludes the diagnosis of PE (recommendation class I). When the CTPA shows segmental or proximal thrombosis in patients with intermediate or high

probability of PE, no further test should be done for the diagnosis of PE (recommendation level I) (2).
The problem when using a CTPA as a diagnosing tool for PE is the radiation exposure and the resultant restrictions involved in its application in pregnant women or young patients. Another main disadvantage is the use of iodinated contrast, because of the risk of hypersensitivity reactions, thyrotoxicosis, and contrast-induced nephropathy (25).

Existing alternatives to the CT scan are lung scintigraphy and pulmonary angiography, both with their own restrictions. The ventilation/perfusion scans use an inhaling contrast agent for ventilation, followed by an intravenous contrast agent for perfusion—both of which are radioactive substances. Further disadvantage is the fact, that no alternative diagnosis can be given if PE has been excluded (2). Pulmonary angiography is an invasive method with its own risks and complications (2). This has led to the need for an alternative imaging modality for the diagnosis of PE, such as MRI, which does not use a contrast agent or expose patients to radiation.

The treatment for PE varies depending on the classification of the PE severity. However, the administration of anticoagulation treatment should immediately be initiated in cases of high and intermediate clinical probability of PE, even without having the final results of the ongoing diagnostic tests (2). The anticoagulation is initiated either with unfractionated heparin (intravenous), low-molecular-weight heparin (subcutaneous), fondaparinux (subcutaneous), or NOACS (non-vitamin K antagonist oral anticoagulants). The treatment of high-risk PE in hemodynamically unstable patients includes a reperfusion treatment, such as systemic thrombolysis with rtPA (recombinant tissue-type plasminogen activator), Streptokinase, and Urokinase (2). After parenteral anticoagulation, oral anticoagulation with NOACS or VTKs (Vitamin K antagonists) follows. Surgical embolectomy or reperfusion percutaneous catheter-directed thrombectomy are existing alternatives if the reperfusion treatment with systemic thrombolysis is contraindicated. A surgical embolectomy can remove a thrombus located up to a segmental branch of an artery. In the case of performing percutaneous catheter-directed reperfusion, thrombectomy can be done by thrombus

fragmentation with a pigtail/balloon catheter, by suction with aspiration catheters, rheolytically with a hydrodynamic catheter, or mechanically by entrapping the thrombus and aspirating it (2,26).

2.2 CTPA and DECT

CTPA is a computed tomography that uses an iodinated contrast to visualize the vascular tree of the lung, which makes it possible to diagnose or rule out a PE. It is the gold standard for the diagnosis (27). In the resulting image, the arteries appear as a bright vascular tree, which means that a structure inside the vessel, such as a thrombus in PE, gives less opacification of the vessel by the radiocontrast.

To understand the function of a CT, the two types of X-rays should be explained briefly. In type one, the characteristic X-rays are produced by the collision of an electron (coming from a negative cathode) with another electron, which is localized in one of the shells of an atom (localized at the positive anode). Thereby, the bound electron is ejected, which leads to occupation by an electron of a higher shell losing energy in the form of a photon (X-ray). This happens when the energy of the incoming electron equals at least the binding energy between the electron positioned in the inner shell and the nucleus. In type two, the electron's path is influenced by the electric field of the nucleus of an atom and thereby energy is emitted in the form of a photon.

The X-rays are radiated on the patient in the form of an X-ray beam. Then, depending on the density and characteristics of the tissue, the X-rays are attenuated more or less. Air is an example of a low density, which consequently appears as a black area in the image. The interaction of the X-rays with the tissue is dominated by two mechanisms: the photoelectric effect, in which the photon is absorbed and the interacting electron emitted, and Compton scattering, a process in which the photon loses energy by being scattered (Figure 4, (28,29)).

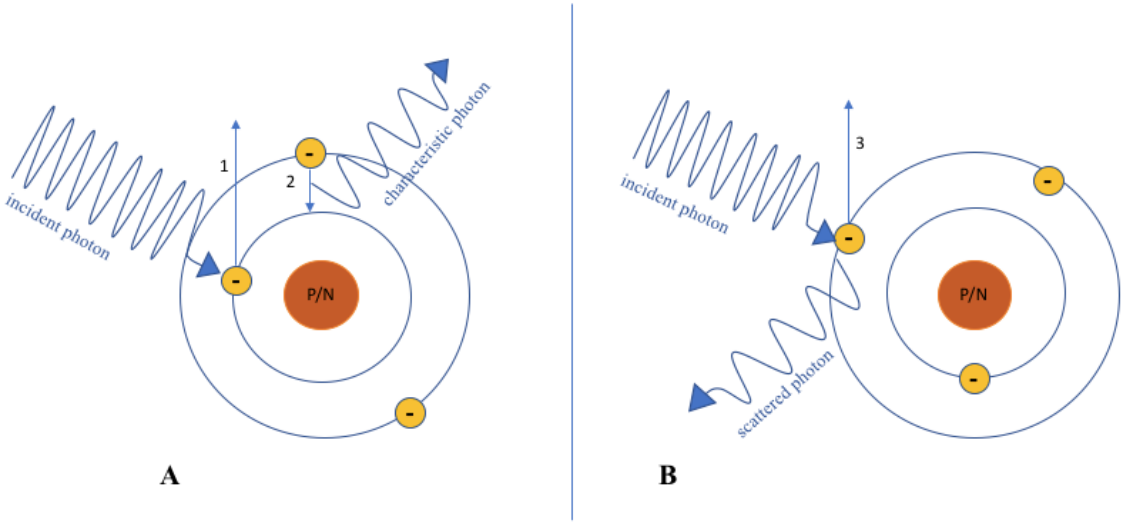

Figure 4: A: photoelectric effect; B: Compton scattering. 1: ejected photoelectron; 2: electron of an outer K-shell fills the gap; 3: ejected photoelectron. The representation follows reference (28,29).

The attenuation of the X-rays is measured as CT values in Hounsfield units (HU), named after Sir Godfrey Newbold Hounsfield. Sir Godfrey Newbold Hounsfield (* 28 August 1919, † 12 August 2004) was an electrical engineer from England who, along with Allan MacLeod Cormack, won the Nobel Prize for Physiology or Medicine in 1979 for their work on X-ray computed tomography (30). The CT value represents a gray level for a specific tissue with a linear attenuation coefficient (μT) relative to the attenuation coefficient of water: $\text{CT value} = (\mu T - \mu water)/\mu water \times 1000$ HU (31). In CT scanners for medical use, the range is between -1024 HU and +3071 HU (31). When displaying a CT image, a window is chosen depending on the tissue of interest. The window means that above and below the chosen Hounsfield units, all values are shown as black or white in the display. This way, the observer can distinguish between the gray levels, since the human eye can only differentiate up to 60 or 80 grey levels, and not 4 096 grey levels (which is the range of the CT values used in medical scanners). For the lung, the window is from -1450 HU to +250 HU, with the center at -600 and a width of 1 700 (31).

One of the main disadvantages of the conventional CTPA compared to a DECT is the lack of functional imaging (32). The DECT works with two X-ray tubes, respectively with two different energies. The mechanism and advantage of this type of CT are based on the different

effects each X-ray energy can have on various substances, depending on the atomic number. When there is an element with a low atomic number, the X-ray photons interact in the form of Compton scattering whereas in substances with a high atomic number the photoelectric effect dominates (33). At a certain energy level, the maximum attenuation is achieved because the incident energy is able to overcome the K-shell (inner-shell) binding energy of the substance (the photoelectric absorption) and thereby ejects an electron. Consequently, the vacancy is occupied by an electron of a higher shell. This peak of attenuation is called the K-edge and is specific for each element. For example, the K-edge values of calcium (4.0 keV) and iodine (33.2 keV) are higher than that of soft tissue (0.01–0.53 keV). The tube with the energy closer to the K-edge attenuates more and hence the attenuation of iodine or calcium is much higher at e.g., 80 kVp than at e.g., 140 kVp (33). The fact that each element has a different K-edge is made use of in DECT.

There are different technical approaches to generating a DECT, and the one used in this study was the Dual-Source CT (a third-generation Dual-Source CT [DSCT], SOMATOM Force, Siemens Healthcare, Forchheim, Germany). The DSCT has two tubes offset by 90 degrees that work simultaneously, and their detectors are located on the opposite side, respectively. Each tube has a different voltage, with one having a smaller field of view due to the position of the two tubes in one gantry (34).

Iodine perfusion map is gained from the datasets of both energy tubes, by applying a dual-energy-postprocessing software in the pulmonary blood volume application mode (35).

When diagnosing a PE, CTPA is the main imaging tool used in practice. The correlation of an embolus seen in the CTPA with the color-coded iodine perfusion maps in DECT was presented in various studies. The study of Fink et al. (8) compared CTPA images with DECT pulmonary angiography in 24 patients with suspected PE. Of these 24 patients, four patients showed a PE in the CTPA and corresponding defects in the iodine perfusion maps of the DECT. Hence, their study concluded that the perfusion maps of DECT enable the detection of perfusion defects caused by PE. The same conclusion was drawn in a study using DECT on 93 patients with suspected PE by Thieme et al. (36).

As explained in the article by Kang et al. (35), a defect of perfusion in the iodine color-coded maps can also occur due to other causes, for example, due to aberrant vessels with a different circulation time, cardiac motion, diaphragm motion, or a lack of contrast material in the superior vena cava.

The general disadvantages of DECT include the higher noise in images obtained by the lower energy tube, the smaller field of view which means that the peripheral areas are not available for dual energy analyses, and the higher radiation dose (35). However, a recent study by Petritsch et al. (7) showed that a lower radiation dose can be achieved in DECT by using a third-generation scanner.

2.3 MRI

MRI is based on the response of hydrogen protons and their magnetic moment to an external magnetic field. Each hydrogen proton rotates around an axis, producing a magnetic field with its own vector (spin). These protons are orientated randomly, but when applying a large external magnetic field (B0), such as the one produced by an MR scanner, the spins become aligned parallel to the B0 direction, i.e., either in direction or in the opposite direction of the B0. Summing up both, it results in a net magnetization ($M \neq 0$) as the majority of spins point in the direction of B0. The B0 direction is also defined as the z-direction, with the x and y directions perpendicular to it. By applying a radiofrequency (RF) pulse, the energy of the RF coil is transferred to the protons with their precession frequency ($\omega 0$), which is also called Larmor frequency, and the direction of the net magnetization rotates to the transverse plane (x-y plane), as illustrated in Figure 5 (37). The frequency of precession $\omega 0$ is proportional to the main magnetic field B0 (Larmor equation: $\omega 0 = \gamma \cdot B0$, with the gyromagnetic ratio of hydrogen γ) (38).

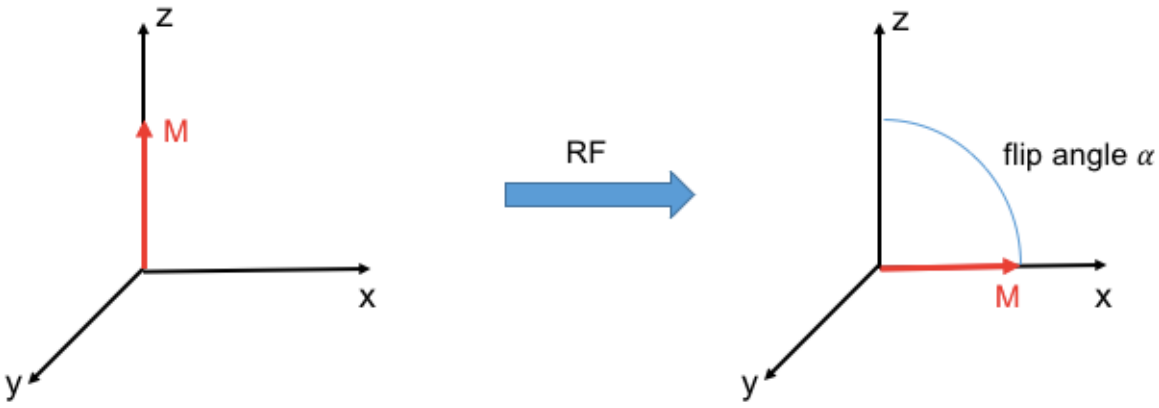

Figure 5: Application of a radiofrequency with the subsequent rotation of the net magnetization to the transverse plane (M: net magnetization; RF: radiofrequency), following reference (37).

When the RF pulse ends, the spins rotate back into their position parallel to the longitudinal axis (the original direction of the net magnetization/z-direction). The relaxation time T1 is

defined as the time needed for net magnetization to reach 63 % of the original value (before the RF pulse) in the z-direction (38). The relaxation time T2 refers to the time after which 37 % of the original value of the net magnetization is left in the transverse plane due to spin dephasing (38). The transverse components of the magnetization induce a signal which is captured by a receiver coil and thereby generates the MR signal, which is also called the free induction decay (38).

To localize the origin of an MR signal in the human body, it is necessary to apply magnetic field gradients. There are three gradients employed for spatial localization of an MRI signal: a slice selection gradient, followed by phase and frequency encoding gradients (38).

During slice selection, a magnetic field gradient (Gz) is applied, which influences the magnitude of the present magnetic field along the defined axis. As a consequence, the precession frequency changes along this dimension, and the spins of each slice perpendicular to it require an appropriate RF pulse frequency to be excited. Exemplarily, this is illustrated for the z dimension in Figure 6 (38). Depending on which axis the slice selection gradient is played out (x, y, or z), a sagittal, coronal, or axial slice orientation is acquired.

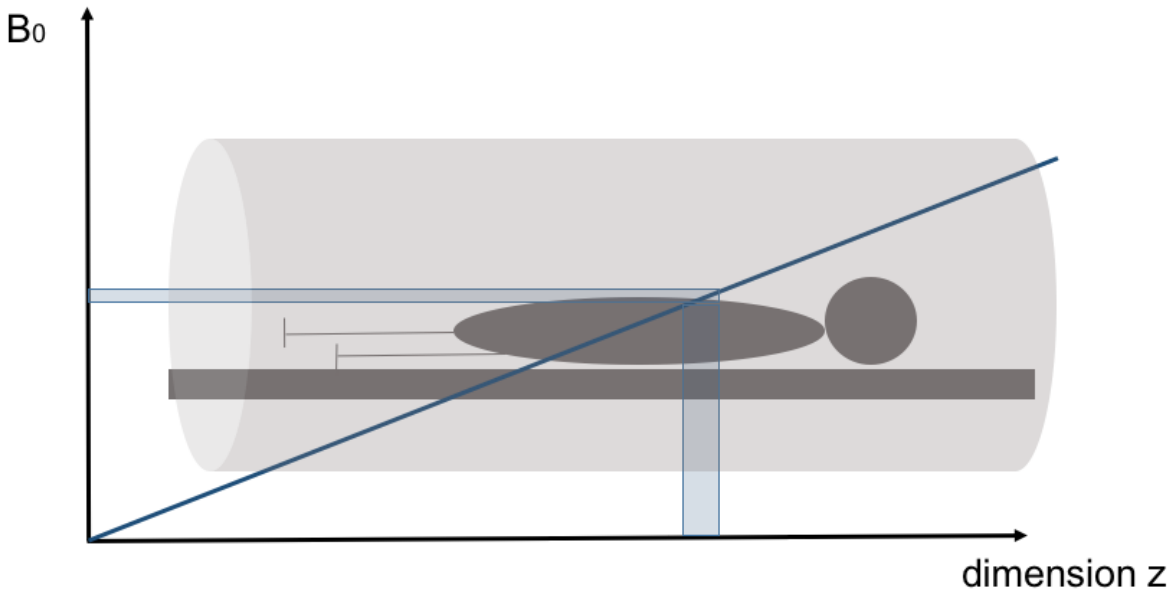

Figure 6: Illustration of the magnetic field gradient strength, with slice selection (blue bars-slice location with a specific magnetic field strength), following reference (38).

If the slice selection gradient is applied e.g., on the z-axis, the localization of the MR signal in the remaining x and y directions is determined by the frequency and phase encoding gradient, respectively. The frequency encoding gradient, which is also called the readout gradient (Gx), is perpendicular to the slice selection gradient (Gz). While the spins in the excited 2D slice precess at the same frequency, they precess at different frequencies along the readout dimension (x) after applying the frequency encoding gradient (Gx). During this time, data acquisition takes place. Before that, the phase encoding gradient (Gy) provides each spin at a unique position along the y-direction with a different phase (Figure 7).

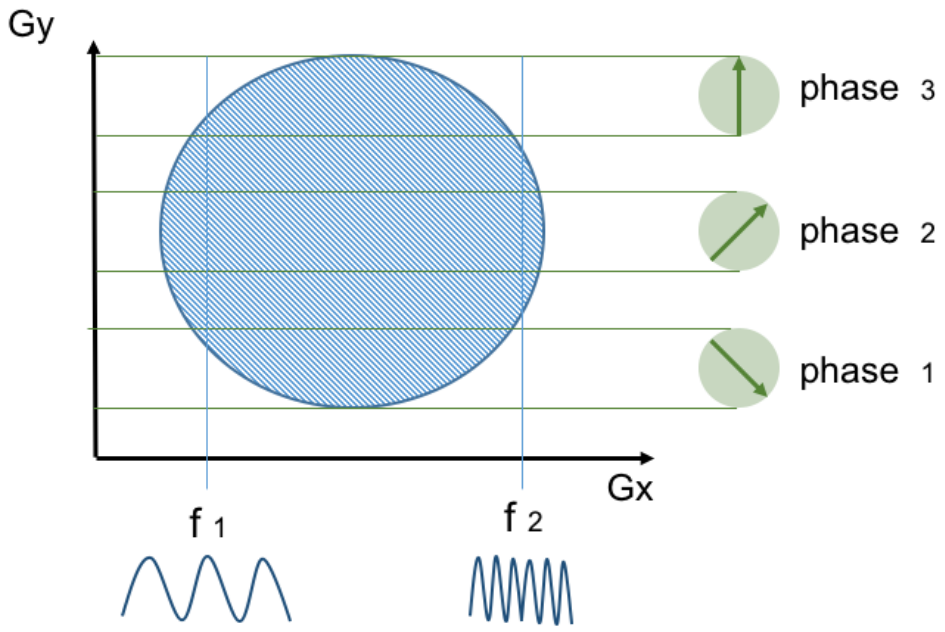

Figure 7: The frequency encoding gradient (Gx) and phase encoding gradient (Gy), following reference (38).

Due to the rapid signal decay in time, a signal echo needs to be created. For this, there are different pulse sequences, such as the spin echo sequence and the gradient echo sequence. In the spin echo sequence, a 180º RF pulse follows the 90º RF pulse to create the signal echo. This type of sequence has the disadvantage that a long imaging time is needed (39). On the other hand, gradient echo sequences, most prominently the fast low angle shot sequence (FLASH), result in short imaging times. By using a low flip angle, less longitudinal magnetization is converted into transverse magnetization and hence the recovery time of the

longitudinal magnetization is shorter, compared to a flip angle of 90° for example.

An exemplary pulse sequence diagram of a FLASH sequence is presented in Figure 8. As described previously, first a slice selection gradient (Gz) is applied, followed by a gradient with negative polarity, also called a compensating gradient. This gradient's duration is half as long as the slice selection gradient since the dephasing occurs in the second half of the slice selection gradient. The phase encoding gradient (Gy) changes its amplitude in each repetition time (TR). The readout gradient (Gx) in a FLASH sequence consists of a reversed polarity, such that the dephased nuclei rephase. This creates a signal echo, which prevents the loss of the MR signal that would normally occur through dephasing in the transverse plane (39).

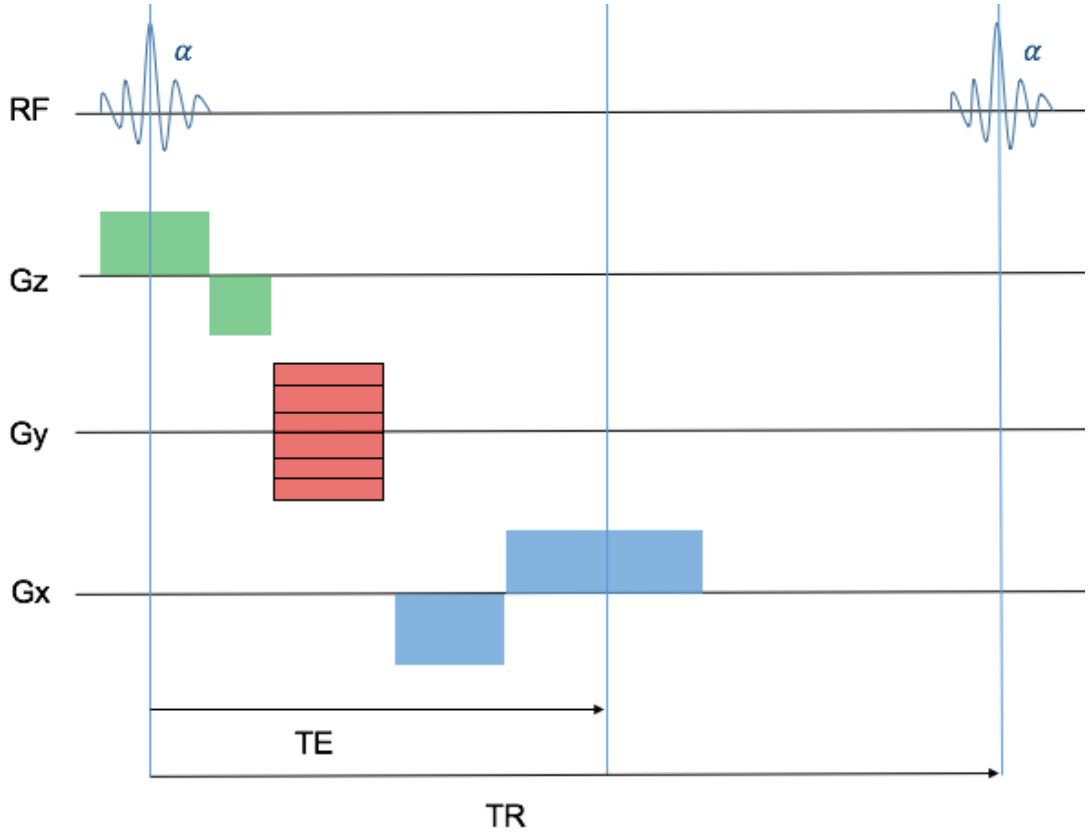

Figure 8: FLASH (fast low angle shot) sequence, following reference (39).

The echo time (TE) is the time from the RF pulse to the signal echo while the TR refers to the time between two consecutive RF pulses.

All the RF signals that are emitted from the various hydrogen protons are measured by a receive coil element. Importantly, the MRI data is acquired in the spatial frequency domain (k-space). By a mathematical procedure called Fourier transform, the information of the k-space is transformed into an image space. One k-space point carries the information of a unique spatial frequency that represents certain structures in the reconstructed image (i.e., spread to multiple pixels in the image space). The information about coarse structures is located in the center of the k-space, whereas that of the more detailed structures is found at the k-space edges.

The main obstacles when performing an MRI of the lung are the low density of protons, the constant movement of parenchyma due to respiration, and the rapid dephasing. Because of this, special technical applications have to be exploited, such as in the SENCEFUL technique, which will be described later on.

In general, there are some limitations when applying an MRI scan. It should not be performed on patients with implanted ferromagnetic foreign bodies, on patients with external electrical devices, and on patients with claustrophobia.

Moreover, it has been indicated that there is a risk of nephrogenic systemic fibrosis related to the use of gadolinium-based contrast agents which is why the creatinine levels and glomerular filtration should be considered when applying these contrast agents. Because of the risk of retention of gadolinium and thus the existence of free gadolinium, it is also recommended that these contrast agents should only be used in pregnant women if strongly indicated (40).

2.4 SENCEFUL MRI

SElf-gated Non-Contrast-Enhanced FUnctional Lung (SENCEFUL) imaging is a technique in pulmonary MRI, which allows for the generation of ventilation- and perfusion-weighted lung maps, without the application of contrast agents or the need for ECG triggering or breath holds during the scan procedure.

According to Fischer et al. (10), the procedure of gaining perfusion- and ventilation-weighted maps is conducted by using a two-dimensional modified FLASH sequence. By applying a lower flip angle, the T1 and T2 times are shortened and, as a result, the TR can also be reduced whereby the data can be acquired more rapidly. In this specific technique, a quasi-random sampling of phase encoding steps is used (10). This means that when applying the phase encoding gradient in each TR, the order of the change in gradient amplitude is not in succession, but random. The sorting of data into the different respiratory and cardiac phases is realized by measuring a non-phase encoded direct current (DC) signal after each readout (self-gating). The DC signal is acquired 20 μs after reading the image data. The respective respiratory and cardiac phases can be reconstructed by including the signal variations when observing certain coils: for respiration a coil near the diaphragm, and for the cardiac cycle a coil near the aortic arch. The DC signal of the coil over the diaphragm reaches its maximum during expiration and its minimum in inspiration. When analyzing the cardiac cycle, the DC signal of the coil near the diaphragm is always in expiration, hence the artifacts due to respiration are reduced.

Subsequently, a pixel-wise Fourier transform along the temporal dimension is performed. In contrast to the standard Fourier Decomposition (FD), the Fourier transform along the temporal dimension in SENCEFUL is used for data modeling only, and by using the first non-zero frequency component, a smooth noiseless image series can be obtained. In this way, the blood flow variations, respectively the signal changes can be depicted semi-quantitatively in the perfusion images.

In general, there are two main advantages of applying this kind of sequence in MRI. Firstly, it is applied during free breathing and no ECG gating is necessary. Since the cooperation for breath control is not always given when respiratory symptoms are present in PE, free breathing is a very important aspect when carrying out the diagnostic imaging. Another advantage is the high spatial resolution (10).

The results of the perfusion- and ventilation-weighted maps with this technique enable a good functional evaluation of the lung, when compared to Dynamic Contrast-Enhanced MRI (DCE-MRI) and standard Fourier Decomposition (FD) (10).

3. Materials and methods

This study aimed to compare the DECT perfusion images and the perfusion-weighted SENCEFUL MR images of the lung with the gold standard for the diagnosis of PE, the CTPA. The study was approved by the ethics committee of the medical faculty of the University of Würzburg. All participants provided written consent prior to imaging.

3.1 Study design

This work is a prospective study of 10 patients with PE diagnosed with dual-energy CTPA. The criteria for inclusion in the study were the depiction of PE in CTPA and that CT was performed on a dual-energy scanner and thus iodine perfusion maps could be calculated from the DECT data. Included patients subsequently underwent SENCEFUL MRI. The iodine perfusion maps of DECT and the images from SENCEFUL MRI were compared to the CTPA. To validate the SENCEFUL MRI and the iodine color-coded maps of DECT as a diagnostic test for PE, the sensitivity, sensibility, and positive and negative predictive values were determined for both functional images. The SENCEFUL MR images and the iodine color-coded maps of DECT were also analyzed on a per-patient basis and compared with each other.

3.2 Study population

The study population comprised patients who underwent treatment at the University Hospital of Würzburg and were diagnosed with a PE by means of DECT-CTPA between June 2016 and January 2017. The study group consisted of four women and six men. The mean age was 60 years, with a standard deviation of 15.8 and the participant age range was from 21 to 80 years. The symptoms of the patients participating in this study, which were reported by the radiologists on duty in the request for CTPA, were most commonly dyspnea (6 of 10 patients). Other signs and symptoms that were described included an increased oxygen demand, thoracic or leg pain, syncope, or cough.

3.3 Study tools

The CTPA images were generated using a third-generation DSCT (Somatom Force, Siemens Healthcare, Forchheim, Germany) with two tube energies of 90/150 kVp. By combining the information from both tubes, an image similar to a conventional CT with 120 kVp was acquired. The perfusion maps were obtained using the DECT. As a contrast agent, iopromide (Ultravist®, Bayer HealthCare), an iodine-based monomeric contrast medium with an iodine concentration of 370 mg/ml, was injected intravenously. The SENCEFUL MRI scans were performed on a 3 Tesla scanner (Magnetom Prisma, Siemens Healthcare, Erlangen, Germany) whereby the following sequence parameters were used: TE: 0.7 ms, TR: 2.5 ms, flip angle: 8 °, field of view: 450 x 450 mm, matrix size: 128 x 128, and slice thickness: 10 mm.

3.4 Data analysis

The following material was used for the comparison of the techniques: CTPA images, iodine color-coded maps calculated from the DECT, and SENCEFUL MR images, as well as the findings written by the radiology reports of the examination. In the SENCEFUL MR images in 5 out of 10 of the studied patients, part of the lung parenchyma, either the frontal or dorsal parts were not shown, because the duration of the examination had to be shortened and focused on the central slices due to the health conditions of the patient.

The data analysis was carried out by one person, a physician. The images acquired with CTPA, DECT, and SENCEFUL MR were analyzed in three steps, which are explained in further detail below. The three steps entailed:

1. The division of pulmonary parenchyma into eight areas per patient (superior frontal right and left, inferior frontal right and left, superior dorsal right and left, inferior dorsal right and left).
2. The determination of each octant as perfused or as a perfusion impairment.
3. The comparison of the diagnostic imaging modalities by using the CTPA scans as the gold standard.

1. Division of parenchyma into eight areas per patient:

The pulmonary parenchyma was divided into octants. For this, the lung parenchyma shown in the CTPA was divided into a frontal (the first half of the images) and dorsal (the second half of the images) section. Afterward, the parenchyma in one of the central layers of the CTPA was divided into superior and inferior parts, and this separation line was kept constant along with the other slices. This subdivision of the lung was transferred to the iodine color-coded maps and SENCEFUL MR images. In Figure 7, one slice of the SENCEFUL MR is shown with its separation into superior and inferior (four) areas (Figure 9).

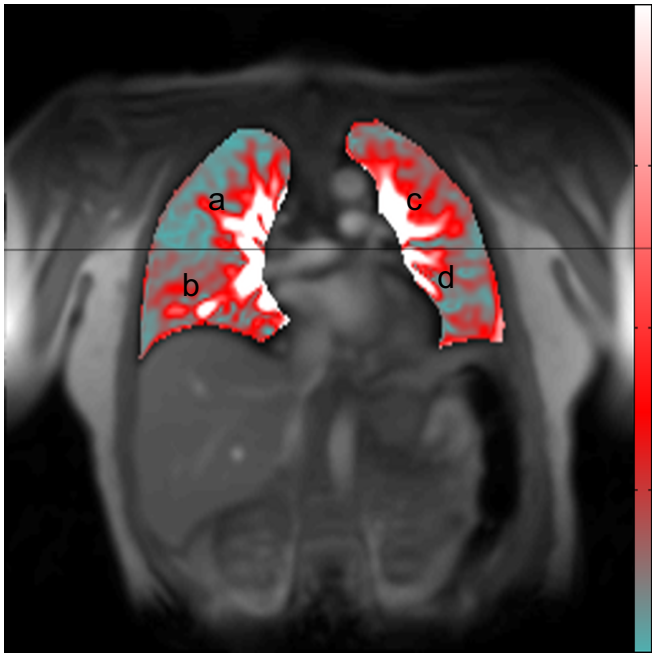

Figure 9: SENCEFUL MRI; a = right superior area, b = right inferior area, c = left superior area, d = left inferior area.

2. Determination of each octant as perfused or as a perfusion impairment:

If one area had a perfusion impairment, the number “1” was noted, whereas if the area was perfused, the number “0” was noted. This data was saved in an Excel table (Microsoft Excel, Redmond, USA). The CTPA images and DECT iodine color-coded maps were viewed using an open-source DICOM viewer (OsiriX Lite, Bernex, Switzerland).

The CTPA reports defined the localization of the PE in the CTPA. Since the thrombus itself is depicted in the CTPA, while the perfusion of the lung is shown in the other two imaging techniques, in the CTPA a conclusion about the perfusion was drawn out of the localization of the embolism. If an octant was affected by thromboembolic material in one of its vessels, this octant was defined as an octant with an expected perfusion impairment. For example, if a central vessel like the right pulmonary artery had an embolism, the four subsequent octants of the right lung were defined as areas with a perfusion impairment (noting number “1” in the Excel table for each of the four octants). As for the SENCEFUL MRI and DECT, each slice of the MRI and the DECT was interpreted with regard to the perfusion, giving each area a number “1” or “0”, depending on whether a perfusion impairment was present or not.

To define one octant of the SENCEFUL MRI and DECT as perfused or as an area with a perfusion impairment, all interpretations of the slices belonging to the defined octant were summarized by counting which number (“1”/“0”) dominates. Figure 10 illustrates the separation of one lung into four octants with the corresponding slices in each octant.

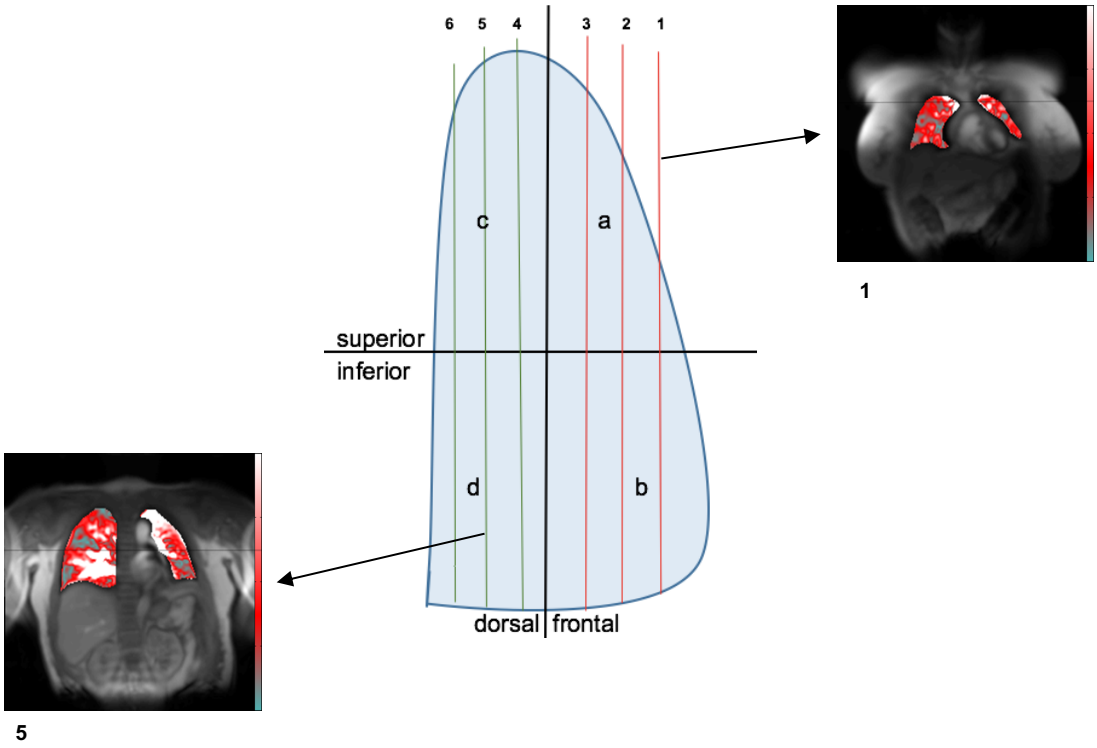

Figure 10: Sagittal view of the right lung half, whereby numbers (1–6) indicate the MRI slices; a = right superior frontal area, b = right inferior frontal area, c = right superior dorsal area, d = right inferior dorsal area. The line that divides the superior from the inferior areas is included in the exemplary images of slices 1 and 5.

3. Comparison of the diagnostic imaging modalities:

Lastly, all octants of the MRI scans and the DECT iodine color-coded maps were compared to our reference, the CTPA, by defining the sensibility, specificity, and positive and negative predictive value using Excel (Microsoft Excel, Redmond, USA) for the calculations.

The functional images were not only analyzed with regard to the different areas but also on a per-patient basis as this approach makes sense for the treatment in the case of PE. All slices of the iodine perfusion maps of DECT and of the SENCEFUL MRI from each patient were

analyzed and a conclusion about the main global lack of perfusion was drawn and compared with each other. If the patient showed a main perfusion impairment due to an embolism, one could have proceeded to the anticoagulation, regardless of the exact location of the thrombus.

4. Results

4.1 CTPA

Our reference test, namely the CTPA of the 10 patients, showed 23 octants that were not affected by thromboembolism and therefore were defined as perfused areas, and 57 octants which – because of the localization of a pulmonary embolism – would consequently have an expected perfusion impairment.

4.2 Iodine color-coded maps of DECT

In the gold standard CTPA, 57 octants were defined as expected perfusion impairments. Of those, 48 octants (84.2 %) were correctly defined as perfusion impairment in the iodine color-coded maps and 9 octants (15.8 %) were false negative. Of the 23 octants defined as perfused in the CTPA, 15 octants (65.2 %) were correctly identified in the iodine color-coded maps, whereas 8 octants (34.8 %) were false positive. A sensitivity of 84.2 % (confidence interval [CI] 95 % 74.7–93.7) and specificity of 65.2 % (CI 95 % 45.8–84.7) were defined for the diagnosis of PE with the iodine perfusion maps of DECT. The positive predictive value was 85.7 % (CI 95 % 78–93.4) and the negative predictive value was 62.5 % (CI 95 % 51.9–73.1) (Table 3).

	CTPA 0	CTPA 1	
DECT 0	15	9	24
DECT 1	8	48	56
	23	57	80

Table 3: CTPA vs. iodine maps of DECT; 0 = no thromboembolic material in CTPA/regular perfusion in DECT iodine maps; 1 = thromboembolic material in CTPA/impaired perfusion in DECT iodine maps.

In Figure 11, the CTPA scan (A) and the functional DECT images in the transversal (B) and coronal orientations (C) of one of the patients are shown. The CTPA scan indicates a lack of opacification of the contrast agent in a segmental artery at the lingula level and the iodine

color-coded perfusion maps of DECT reveal a defect of perfusion in the lingula. The perfusion defects shown in Figure 11 are highlighted by white arrows, respectively.

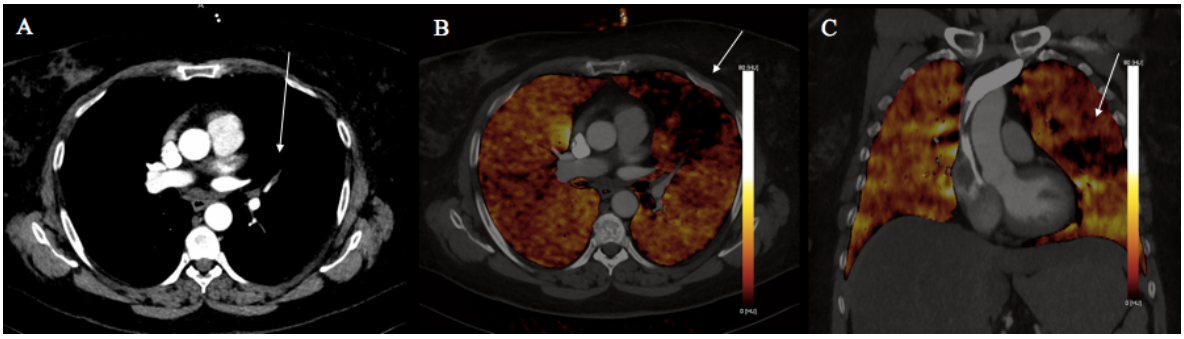

Figure 11: A: CTPA scan with PE in segmental artery lingula level; B and C: perfusion maps of DECT slices with visible defect of perfusion in transversal (B) and coronal (C) orientation.

4.3 SENCEFUL MRI

When rating the octants in the SENCEFUL MR images, 18 were interpreted as perfused areas, while 62 showed impaired perfusion. In the CTPA, 57 octants were affected by a thrombus with a consequent perfusion impairment and 23 octants had no thromboembolic material and were interpreted as perfused. Of the 57 octants with expected impaired perfusion due to the embolism, 45 areas (78.9 %) were also interpreted as perfusion impaired in the MR images, 12 octants (21.1 %) were false negative. In the case of the 23 perfused areas, six octants (26.1 %) were also described as perfused in the MR images, 17 octants (73.9 %) were false positive (Table 4).

	CTPA 0	CTPA 1	
SENCEFUL 0	6	12	18
SENCEFUL 1	17	45	62
	23	57	80

Table 4: CTPA vs. SENCEFUL MR techniques, 0 = no thromboembolic material in CTPA/regular perfusion in SENCEFUL MRI; 1 = thromboembolic material in CTPA/impaired perfusion in SENCEFUL MRI.

To validate the SENCEFUL technique in MRI as a diagnostic test, the sensitivity and specificity were determined. This study observed a sensitivity of 78.9 % (CI 95 % 68.4–89.5) and a specificity of 26.1 % (CI 95 % 8.1–44) in the diagnosis of PE whereby the results show that the sensitivity is higher than the specificity which means that the probability that a patient with a PE, who has a perfusion impairment, shows a defect of perfusion in the SENCEFUL MRI is 78.9 %. However, the probability that a patient who really has no defect of perfusion according to the CTPA, has a SENCEFUL MRI with perfused areas is 26.1 %. The positive predictive value of the MR images was 72.6 % (CI 95 % 62.8–82.4) and the negative predictive value was 33.3 % (CI 95 % 23–43.7). Figure 12 shows two slices of the CTPA scan of one of the patients with a thrombus in both right and left main arteries (a and b), and two corresponding slices of SENCEFUL MRI with the depicted defect of perfusion in the right and left lung (c and d).

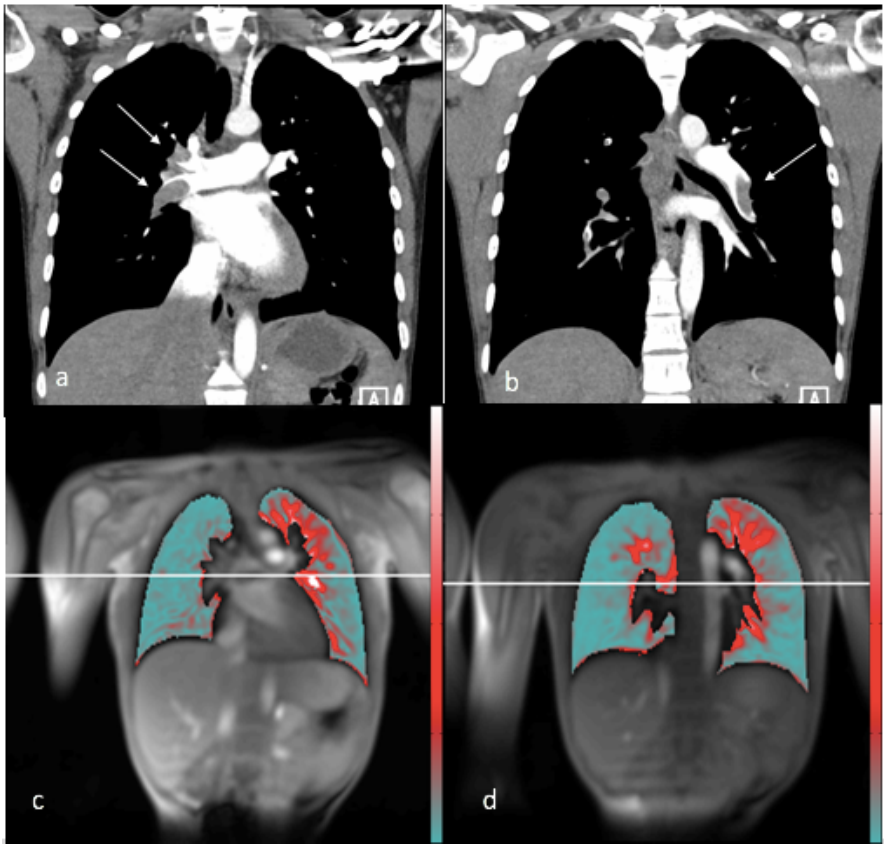

Figure 12: CT slices (a and b) vs. SENCEFUL MRI (c and d). Localization of the embolism highlighted with white arrows.

4.4 SENCEFUL MRI and iodine color-coded maps of DECT

All 10 patients of this study, who were diagnosed with PE in the CTPA, showed perfusion impairments in both functional images. Comparing the iodine color-coded maps of DECT and the SENCEFUL MR images with each other on a per-patient basis, it was observed that in four of 10 patients (40 %) the conclusion about the main perfusion defect location matched, whereas in six of 10 patients (60 %) the main perfusion impairment shown in the iodine color-coded maps did not correspond to the one in the perfusion maps of SENCEFUL MRI. In Figure 13, an example of one of the four patients is shown, in which the main localization of a perfusion impairment matched in both functional images.

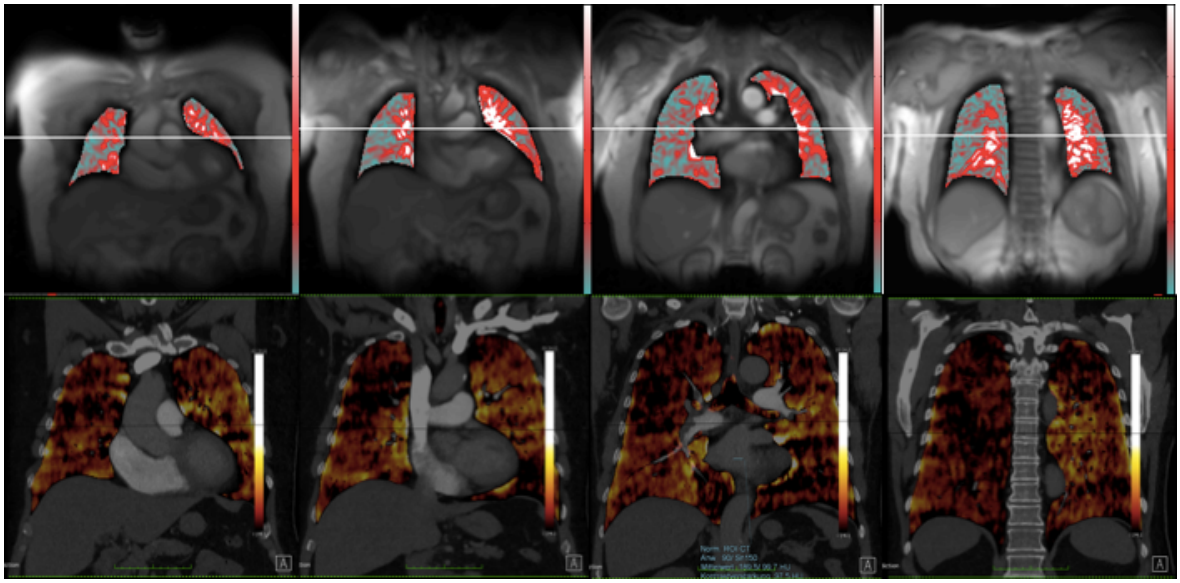

Figure 13: Four slices of SENCEFUL MR (first row) vs. four corresponding slices of iodine maps of DECT (second row) of the same patient; left to right = frontal to dorsal. The maps show a perfusion impairment mainly in the right lung half, in particular the right superior lobe.

While the extent of the perfusion defect shown in the functional images of the four patients was not always the same in the two corresponding functional images, the main localization matched, as shown in Figure 14.

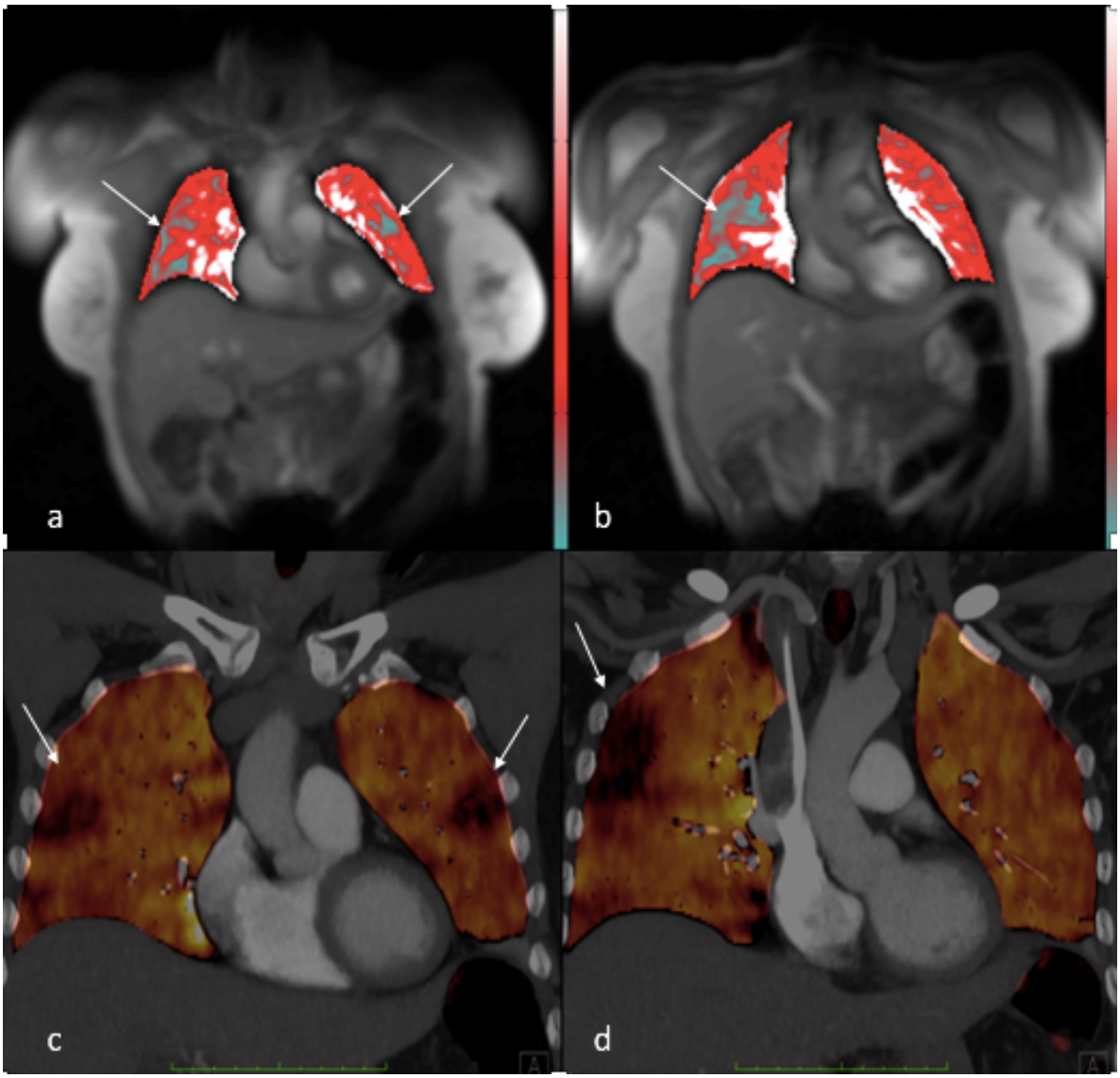

Figure 14: a and b: SENCEFUL MR Images; c and d: corresponding iodine perfusion maps DECT. The maps of SENCEFUL MRI and iodine maps of DECT show a perfusion impairment in the right superior/middle lobe, as well as in the left superior lobe in the frontal layers (highlighted by white arrows). The extent of the perfusion impairments, shown in blue in SENCEFUL MRI and in black in the iodine maps of DECT, have not the same size.

5. Discussion

This study aimed to determine whether PE can be diagnosed on the basis of visible perfusion defects in perfusion maps of SENCEFUL MRI and iodine color-coded maps of the DECT. They were analyzed by octants and compared to the gold standard in diagnosis of PE, the CTPA. The sensitivity, specificity, and positive and negative predictive values of both functional images were defined. Additionally, the two perfusion maps of the functional images were compared with each other on a per patient-basis.

The sensitivity is the ratio between the correctly identified perfusion impairments shown in the DECT or SENCEFUL and all perfusion defects shown in the CTPA and it describes the probability that a perfusion impairment is successfully identified in the DECT or SENCEFUL MRI. The specificity refers to the correctly identified perfused areas of all perfused areas shown in the CTPA and the positive predictive value refers to the probability that a perfusion impairment shown in the DECT or SENCEFUL MRI corresponds to a truly existing lack of perfusion in the patient. It is thus the ratio between the correctly identified defects of perfusion and all observed defects of perfusion in the DECT or SENCEFUL MRI. The negative predictive value is the probability that a negative result, meaning a completely perfused area of the lung, is truly perfused in the patient's lung.

The iodine color-coded maps of DECT had a sensitivity of 84.2 %, a specificity of 65.2 %, a positive predictive value of 85.7 %, and a negative predictive value of 62.5 %. The SENCEFUL MRI showed a sensitivity of 78.9 %, a specificity of 26.1 %, a positive predictive value of 72.6 %, and a negative predictive value of 33.3 %.

The sensitivity of both imaging tools was approximately 80 %, which means that the iodine color-coded maps of the DECT and SENCEFUL MR images identified the perfusion impairments due to the PE shown in the CTPA with a rather good probability. As the specificity was rather low, in particular in the SENCEFUL MRI, the perfused areas were not identified correctly. The positive predictive value was high in the iodine color-coded maps, which means that impaired perfusion corresponds to an existing lack of perfusion. Concurrently, the negative predictive value, again of the SENCEFUL MRI in particular, was very low.

The sensitivity and specificity of the iodine perfusion maps of DECT were higher than those of the SENCEFUL MR images for the diagnosis of PE, which means that the iodine perfusion maps of DECT have a higher validity as a diagnostic test.

When comparing the whole lung and the localization of the main perfusion impairment, in four of 10 patients (40 %) the iodine maps of the DECT and the SENCEFUL MR images matched. When assuming that the thrombus is localized in the same vessel, this is a rather low percentage. However, it should be considered that the MRI was carried out after the DECT and, during this time, the localization of a PE could have changed.

The diagnostic imaging for PE can be provided by MRI, CTPA, scintigraphy, single-photon emission computed tomography, positron-emission tomography, or pulmonary angiography. In CTPA, functional perfusion images can be obtained by applying a dual-energy protocol. DCE-MRI (41), arterial spin labeling (ASL-MRI) (42), and standard Fourier decomposition with steady-state precession (SSFP) pulse sequence (43) or the SENCEFUL technique with a fast low-angle shot (FLASH) sequence (10) are different existing approaches in MRI. In the depiction of the lung parenchyma, DECT and MRI have both advantages and disadvantages. The main disadvantage of DECT is the radiation exposure and the use of contrast agents. Radiation exposure is defined in terms of deterministic and stochastic effects, which refer to the direct damage of a certain tissue and to cancer induction or genetic effects respectively. The adverse reactions resulting from the use of iodinated contrast agents mainly include hypersensitivity reactions, thyrotoxicosis, and – more importantly – contrast-induced nephropathy (25). It is essential to develop alternative diagnostic tests for PE, such as MRI, that do not use X-rays or iodinated contrast agents. The imaging of the pulmonary parenchyma with MRI is challenging as MRI is based on protons reacting to a magnetic field, and the lung is an organ with a very low density of protons. Moreover, the interfaces between air and tissue in the alveoli produce magnetic field inhomogeneities which cause rapid dephasing and result in a fast signal decay, which is another obstacle that needs to be considered in MR imaging. Additionally, the constant movements due to the respiratory and cardiac cycle with blood flow are causes of artifacts in the resultant images produced. One

important advantage of SENCEFUL MRI for patients with a PE, who can exhibit respiratory symptoms like dyspnea, is the fact that they can be conducted in free breathing. In contrast to other existing MR approaches, in SENCEFUL no apneas need to be performed. Since the patient's noncompliance with breath holds can be the main obstacle when performing diagnostic imaging tests, an approach without the need for breath holds would be easier to realize in practice and increase the patient's comfort.

At present, one of the main studies concerning the diagnosis of PE is the Prospective Investigation of Pulmonary Embolism Diagnosis II (PIOPED II) (3), and therefore the results obtained in the present study will, among others, be compared to the findings from the PIOPED II study.

The PIOPED II showed a sensitivity of 83 % and a specificity of 96 % for the diagnosis of PE with CTPA, excluding the inconclusive images (3). In combination with venous phase imaging, the sensitivity was higher (90 %), and the specificity was similar (95 %). Moreover, the importance of the clinical assessment, in addition to the imaging modality in the diagnosis of PE, is given by the high positive or negative predictive value when considering the clinical probability in the diagnosis of PE with CTPA. The positive predictive value was higher the more centrally the affected vessel was located, in lobar PE 97 %, while in the sub-segmental PE 25 % (3). Concluding from this study, an additional imaging tool enables a higher sensitivity, which also resulted from the Prospective Investigation of Pulmonary Embolism Diagnosis study III (PIOPED III) (44). The sensitivity and specificity of the iodine maps of DECT in the present study were 84.2 % and 65.2 %, respectively. In the PIOPED study II, a similar sensitivity was observed with CTPA, but a much higher specificity than in the iodine perfusion maps of DECT in the present study (3). The SENCEFUL MRI showed a sensitivity of 78.9 %, a specificity of 26.1 % in this study, and compared to PIOPED II a lower sensitivity and in particular, a lower specificity was determined.

Standard CTPA localizes the thrombus but does not give functional information about the lack of perfusion. The DECT allows a representation of the vascular tree of the lung as well as the perfusion of the lung parenchyma with the iodine maps. The combination of two tube

energies, 90/Sn150 kV, gives a more detailed tissue description (7). By applying a 90 kV tube potential and thus being nearer to the k-edge of iodine, the attenuation is higher. According to the study by Petritsch et al. (7), the diagnosis of PE with DECT scans has the advantage of providing good image quality, including perfusion maps with a lower radiation dose compared to the single-source CT scans (DECT -2.79 mSv versus DSCT single energy -4.24 mSv and Single-Source CT [SSCT] at 120 kV–4.6 mSv). The volume computed tomography dose index, dose length product, and effective dose were shown to be lower in the dual-energy protocol than in the single source protocol (7).

In a study on six rabbits that underwent pathologic analysis (reference for the diagnosis of PE in this study), Zhang et al. (45) reported a sensitivity of 67 % and a specificity of 100 % using CTPA. The sensitivity of the perfusion maps gained by contrast-enhanced DECT was 89 % and the specificity 92 %. With these results, they concluded that the DECT scans improved the detection of PE. The feasibility of DECT in the diagnosis of PE was also presented in a study by Fink et al. (8). Of the 24 patients examined, four showed a PE in the CT, which was used as the reference test. According to the two radiologists, the sensitivity and specificity of the perfusion maps of DECT for the diagnosis of PE on a per-patient basis was 100 %, whereas the sensitivity on a per-segment basis was between 60 and 66.7 %, and the specificity between 99.5 and 99.8 %.

When compared to the PIOPED II study (3) and that of Zhang et al. (45), the sensitivity and specificity of the iodine maps of the DECT and the SENCEFUL MR images in the present study are lower which means that the perfused and impaired perfused areas are not recognized as accurately as in other studies. This could be due to the fact that four out of 10 patients studied had a thrombus in both main pulmonary arteries. When the thrombus was localized in both main pulmonary arteries, all corresponding eight areas of the lung were interpreted as areas with an expected perfusion impairment in the CTPA, while in the corresponding iodine maps of the DECT and the SENCEFUL MR, images with perfused areas were described. This could be because of remaining perfusion related to an incomplete opacification of the main vessel due to the thrombus. However, since in the CTPA, all areas

were defined as areas with a perfusion impairment, the sensitivity and specificity of the iodine maps of DECT and the SNECFEUL MRI were lower. In the study on rabbits (Zhang et al. (45)), a pathological analysis was performed as a reference examination. The CTPA as a gold standard is not as precise as the pathological analysis, small embolisms in the periphery of the lung could have been overseen in the CTPA, as contrast to the pathological analysis. This could be one of the reasons for the different specificity, even though it would not explain the higher sensitivity observed in the present study.
In the study by Fink et al. (8), the sensitivity and specificity of the perfusion maps of DECT were higher on a per-patient basis than on a per-segment basis. In the present study, the lung was divided not into segments, but into octants and the sensitivity of the perfusion maps of the DECT is higher compared to the results on a per-segment basis of the study by Fink et al., while the specificity is much lower.

Many approaches have been presented within the MRI spectrum for functional imaging of the lung including DCE-MRI (41), ASL-MRI (42), standard Fourier decomposition (43), and the SENCEFUL technique (10). The ASL-MRI, standard Fourier decomposition, and SENCEFUL are alternatives that yield no-contrast-enhanced functional images.
The DCE-MRI is an MRI technique that applies intravenous gadolinium contrast agent in e.g. a gradient echo sequence (41). The data is acquired during the patient's breath hold. As mentioned, the use of gadolinium-based contrast agents can produce allergic reactions, and nephrogenic systemic fibrosis has been described in connection with the use of such contrast agents (40). The ASL-MRI technique is an approach that uses magnetically labeled blood water as contrast (42). In this procedure, the images were acquired with ECG triggering and breath holds to minimize the artifacts. When compared to the study presented in this thesis, the main advantage of the SENCEFUL MRI is the lack of a contrast agent and the possibility of free breathing during the examination.

Bauman et al. (43) presented another approach for functional imaging of the lung with MRI, in which neither contrast agent, apnea, nor ECG triggering was needed. The ventilation- and perfusion-weighted maps were prepared by applying a two-dimensional true fast imaging

with a steady precession (True FISP) pulse sequence (43). In the True FISP pulse sequence, the magnetization was refocused within each TR by balancing all applied magnetic field gradients. The images were optimized by applying an asymmetric echo sampling and parallel imaging in a 1.5T system. In the study, Fourier decomposition was introduced to quantify ventilation and perfusion. The Fourier analysis was conducted in the temporal frequency dimension, in which two frequencies, one for the respiratory and one for the cardiac dynamics, were observed in a region of interest. By applying a nonrigid registration algorithm, the changes in the lung due to respiration were rectified and a reference image was chosen. Three images per second were obtained with a matrix size of 128 x 128 and a parallel imaging factor of three. The flip angle α was achieved by 10 preparation pulses, which means that the flip angle was increased step by step until reaching α. This was done to improve the stabilization of the magnetization vector. In this study, three volunteers and two patients were examined, of whom one patient was diagnosed with a cystic parenchymal defect and one with a PE. Both the parenchymal defect and the lack of perfusion could be detected in the patient's images. One main disadvantage of this approach is that the breathing and the cardiac rates need to be stable as, in cases where these are irregular, the spectral lines are broadened thereby resulting in more noise in the images (43).

On the contrary, instead of balancing the moments, a spoiled gradient echo was used in the SENCEFUL technique, which means that the residual magnetization is destroyed after each data acquisition. Another main difference between both studies is the self-gating procedure. In the SENCEFUL technique, a non-phase-encoded direct current (DC) signal was acquired in each TR. Moreover, a high resolution could be achieved using the SENCEFUL technique with an image matrix size up to 256 x 256 (10).

The multicenter prospective study (PIOPED III) investigated the gadolinium-enhanced MR angiography for PE (44) whereby a group of 371 adults underwent MR angiography and venography. Compared to the reference diagnostic tests (e.g., CT, ventilation/-perfusion lung scans, ultra-sonography), the MR angiography showed a sensitivity of 78 % and a specificity of 99 %. When including the venography, the sensitivity for diagnosing a PE was 92 % and

the specificity 96 % (44). These data refer to the technically adequate images. In a range of 11–52 %, the images of MR angiography were technically inadequate (44).

In the IRM-EP study (46), a group of 300 patients, who were examined with CTPA because of suspected PE, additionally underwent an MRI with unenhanced perfusion and angiographic sequences. Of the 300 patients, 274 MRI results were studied, and in 103 patients a PE was confirmed by CTPA. The sensitivity of the MRI depended on the reader's interpretation between 78.7 % and 84.5 %, and the specificity lay between 99.1 % and 100 %, excluding the inconclusive MRI results and including sub-segmental PE in the reference (46). As seen in other studies of the pulmonary vascular tree affecting PE, here, a higher sensitivity also resulted from a more proximal location of the affected vessel. The difference in sensitivity according to the localization of the thrombus was 97.7 % to 100 % in proximal vessels, and 21.4 % to 33.3 % in sub-segmental vessels (46).

Compared to the IRM-EP study (46) and the PIOPED III study (44), the sensitivity of both SENCEFUL MRI and iodine color-coded maps of this study were similar, but the specificity was much lower, in particular in the case of the SENCFEUL MRI. As mentioned, this discrepancy in the results could be because of the conclusions drawn by the interpreter when analyzing the CTPA and defining the expected perfusion impairments. Even though in the CTPA it was concluded that in the corresponding octant of localization of a thrombus an impairment of perfusion would exist, an incomplete opacification of the artery by a thrombus could have shown no restriction in the perfusion which could subsequently have affected the sensitivity and specificity. Furthermore, the CTPA as a reference test could have overseen small embolisms in the periphery of the lung, which could have influenced the sensitivity and specificity of both functional imaging procedures.

The sensitivity and specificity of SENCEFUL MRI could also have been affected by the inclusion of the MR images at the edge of the lung with a partial volume effect, which was interpreted as areas with a perfusion impairment. The partial volume effect will be discussed further in the limitations of this study. If these images at the edge of the lung would have

been excluded, higher sensitivity and specificity could have been achieved. It should also be noted that the SENCEFUL MR images were obtained after the CTPA scans, and hence, during this time interval, the expansion of the thrombus could have changed, and respectively the perfusion. This could have affected the discrepancy in the statistics between the CTPA, the iodine color-coded maps of the DECT, and the MRI. In addition, the depiction of the blood vessels and the corresponding high perfusion could have led to a misinterpretation of the perfusion of the parenchyma itself. If the main blood vessels would be excluded from the perfusion map, perhaps a clearer statement could be made from the functional images in SENCEFUL MR and iodine color-coded maps of the DECT. Another key aspect to take into consideration is the use of a contrast agent in the iodine color-coded maps of DECT. The SENCFEUL MRI did not use any contrast agent, which could also affect the accuracy of the depiction of the perfusion and be a further source of the discrepancy in the statistical values between both functional images.

Generally, a diagnostic test with high sensitivity can be useful when ruling out a disease since the false negative rate (incorrectly defined perfused areas) is low (sensitivity + false negative rate = 1). This is why, in the case of a perfused area in the MR images or iodine maps of the DECT, it is unlikely that it corresponds to an area affected by a thrombus.

In clinical routine, a test with high sensitivity can be very helpful. Before using imaging tools with radiation and contrast agents to confirm the disease, such as the CTPA, the MRI could serve as a preliminary screening test to rule out the disease. A patient with perfusion maps of SENCEFUL MRI that do not show any perfusion impairments, would not need to have further tests, especially not any that use radiation and contrast agents. By including the clinical probability in this diagnostic path, the probability to overlook perfusion impairments would be lower. Another possibility to achieve higher sensitivity in SENCEFUL would be an additional test, e.g., an ultrasound of the lower limbs, as shown in other studies.
The very low specificity in the SENCEFUL MR approach means that when applying this technique, the perfused areas are not always identified correctly. Consequently, SENCEFUL imaging would not be a good alternative to confirm the disease. Although the specificity of

the DECT iodine maps is higher than that of the SENCEFUL images in the present study, it is not sufficiently high to rely on it as a confirming imaging tool.

In conclusion, the iodine color-coded maps of DECT offer higher sensitivity and specificity than the SENCEFUL MRI for the diagnosis of PE. However, considering that the SENCEFUL MRI does not use any radiation, it showed a good sensitivity for the diagnosis of PE which is why this imaging tool could be useful in the diagnostic path of a PE, for example as a test before applying a CTPA. To be able to use SENCEFUL as the only imaging tool for the diagnosis of PE, the technique needs to be further improved.

6. Study limitations

In the following, certain limitations of this study will be discussed. Firstly, one important limitation in this study was the CTPA itself as a reference test. The expected perfusion impairment as conclusion of the localization of the thrombus shown in the CTPA could be incorrect, since a not total opacification of the artery could have led to a perfusion in one octant even though it was interpreted as not perfused. Another main limitation is the fact, that in the CTPA small embolisms in the periphery of the lung could have been overseen. These limitations influence negatively the sensitivity and specificity of the functional techniques.
Considering the SENCEFUL MR images, part of the lung was not depicted in the images, and in the existing images, the partial volume effect may have influenced the overall interpretation. In five of the 10 patients, part of the lung parenchyma, either the frontal or dorsal parts was not shown, because the examination had to be shortened and focused on the central slices due to the health conditions of the patient at the time of the screening. Another aspect was the presence of a partial volume effect on the edges of the thorax, as shown in the following images of one patient. As demonstrated in Figure 15, a change from a mainly perfused to a non-perfused area was observed in the dorsal part of the lung. The last slice (b) is depicted completely in blue (no perfusion), and the slice before it (a) is predominantly perfused. This is an example of the partial volume effect at the edge of the lung.

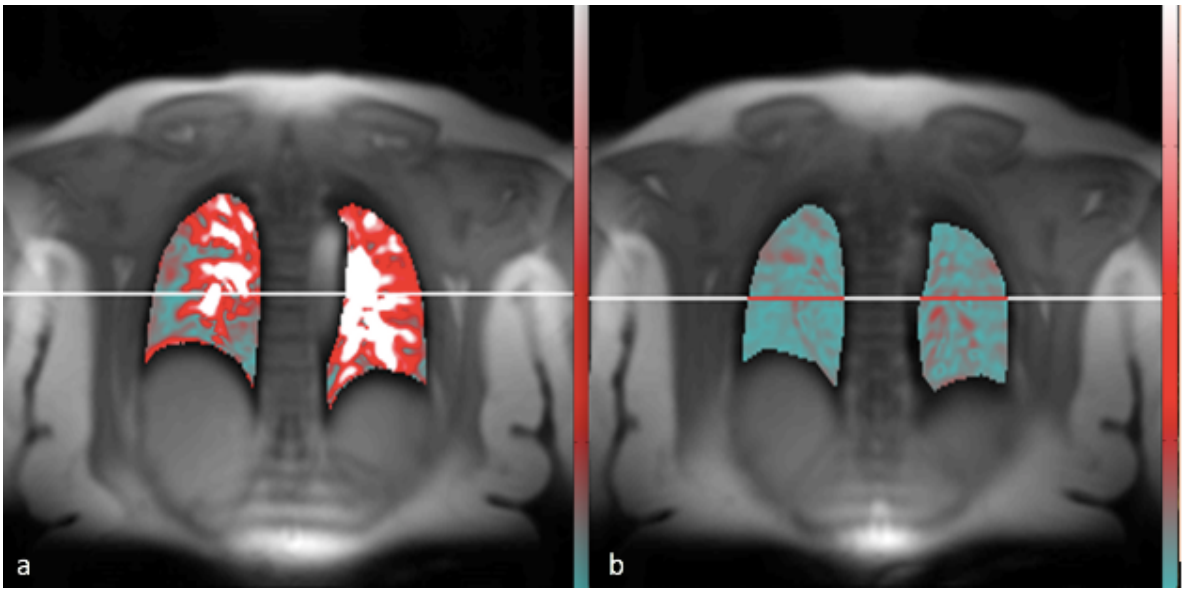

Figure 15: SENCEFUL MRI, two subsequent dorsal slices, a: predominantly perfused, b: complete lack of perfusion.

These limitations in the SENCEFUL MRI could explain the lower sensitivity and specificity in the MR images compared to the iodine color-coded maps of DECT in this study.

Furthermore, the interpretation of the DECT iodine maps and the MRI perfusion maps was performed by one observer only, which means that it was not possible to investigate the interobserver variability. The interpretation of the perfusion impairments is subjective, i.e., reader dependent, and an objective procedure would increase the reproducibility. In a study of 34 cystic fibrosis patients in which unenhanced Fourier decomposition MRI and DCE MRI were performed, in conjunction with specialized software two readers defined the perfusion impairments (47). The software enabled the quantification of the perfusion defects in terms of percentages, which increased the precision compared to the visual analysis. The lungs were divided into three areas from apical to basal, and pixel values were used to define the percentage of perfusion impairments. However, in the automated analysis of the perfusion maps, the inter-reader agreement with the visual analysis was inferior to the inter-reader agreement between two visual readers, because of problems in the segmentation procedure or voxel distribution (47).

Another limitation of this study is the small group size. Consequently, the findings cannot be extrapolated to all patients suffering from a PE. Moreover, the observer in the study is a physician but not a radiologist, which could have had an impact on data interpretation due to limited experience in the field of radiology. Lastly, the study participants were all patients with a diagnosed PE and no images of healthy persons without a PE were included in the analysis and comparison.

7. Summary

In this study, the iodine perfusion maps of DECT and the SENCEFUL MRI of 10 patients diagnosed with PE were compared to the gold standard of PE, the CTPA. For this purpose, the lung of each patient was divided into octants, and the sensitivity, specificity, and positive and negative predictive values of each functional imaging modality were determined. Additionally, both functional images were compared with each other on a per-patient basis.

The iodine perfusion maps of DECT had a sensitivity of 84.2 % (CI 95 % 74.7–93.7) and specificity of 65.2 % (CI 95 % 45.8–84.7) for the diagnosis of PE. The positive predictive value was 85.7 % (CI 95 % 78–93.4) and the negative predictive value was 62.5 % (CI 95 % 51.9-73.1). The SENCEFUL technique in MRI showed a sensitivity of 78.9 % (CI 95 % 68.4–89.5) and a specificity of 26.1 % (CI 95 % 8.1–44) while the positive predictive value of the MR images was 72.6 % (CI 95 % 62.8–82.4) and the negative predictive value 33.3 % (CI 95 % 23–43.7). When comparing the whole lung depicted in both series of functional images, the main perfusion defect location matched in four of 10 patients (40 %).

The iodine perfusion maps of DECT were shown to have a higher sensitivity and specificity than the SENCEFUL MRI in the diagnosis of a PE. This could be due to the existing contrast agent in the DECT, which could have led to a more exact perfusion map, but also be due to the disadvantages of lung MRI itself, i.e., the low proton density, and the magnetic field inhomogeneities, and the artifacts due to motion. Moreover, due to the rather long examination times in MRI and the poor health condition of the patients at the time of examination, the MR images in this study did not always depict the whole lung which also could have affected the sensitivity and specificity of the results obtained. The sensitivity and specificity in both perfusion imaging tools could also have been affected by the localization of the PE in both main pulmonary arteries. In this case, all areas in the CTPA were defined as areas with a perfusion defect, while the functional images also showed perfused areas. The expected perfusion impairments could have been incorrect, since a not total opacification of the vessel could have led to a remaining perfusion. The CTPA as a reference test could also

have overseen small embolisms in the periphery of the lung, which could have affected the sensitivity and specificity of the functional imaging techniques in this study.

Furthermore, it should be considered that MRI does not use any radiation or contrast agent and is done in free breathing whereby the increased level of radiation exposure in modern clinical practice is a very important aspect in this matter since the diagnosis of PE is often done by CTPA.

In conclusion, this work found that DECT iodine maps have higher sensitivity us specificity in the diagnosis of pulmonary embolism compared with SENCEFUL MRI.

8. Zusammenfassung

In dieser Studie wurden DECT Iodkarten und SENCEFUL MRT Bilder von 10 Patienten mit diagnostizierter Lungenembolie mit dem Goldstandard, dem CT, verglichen. Jede Lunge wurde in acht Areale eingeteilt und alle Areale der Iodkarten und der MRT Bilder wurden mit dem CT verglichen. Die Sensitivität, Spezifizität, der positive und negative prädiktive Wert der jeweiligen funktionellen Bildgebung wurden bestimmt. Außerdem wurden beide funktionelle Bildgebungstechniken miteinander verglichen, indem die Hauptperfusion beurteilt wurde.

Die Iodkarten hatten eine Sensitivität von 84.2 % (CI 95 % 74.7-93.7) und eine Spezifizität von 65.2 % (CI 95 % 45.8-84.7). Der positive prädiktive Wert war 85.7 % (CI 95 % 78-93.4), der negative prädiktive Wert 62.5 % (CI 95 % 51.9-73.1). Die SENCEFUL MRT Bilder zeigten eine Sensitivität von 78.9 % (CI 95 % 68.4-89.5) und eine Spezifizität von 26.1 % (CI 95 % 8.1-44). Der positive prädiktive Wert lag bei 72.6 % (CI 95 % 62.8-82.4) und der negative prädiktive Wert bei 33.3 % (CI 95 % 23–43.7). Der Vergleich beider funktioneller Bildgebungstechniken bezogen auf die gesamte Lunge ergab, dass in vier von 10 Patienten die prädominierende Lokalisation der Minderperfusion übereinstimmte.

Die Iodkarten zeigten eine höhere Sensitivität und Spezifizität als die SENCEFUL MRT Bilder. Eine Ursache hierfür könnte die Anwendung eines Kontrastmittels in den Iodkarten sein, welche zu einer genaueren Abbildung der Perfusion führen könnte. Darüber hinaus hat das MRT als Bildgebung der Lunge einige Nachteile, wie beispielsweise eine geringe Protonendichte, Magnetfeldinhomogenitäten und Bewegungsartefakte. Aufgrund limitierter Aufnahmezeiten beim MRT konnte nicht bei allen Patienten die komplette Lunge abgebildet werden, was ebenfalls die Sensitivität und Spezifizität der MRT beeinflusst haben könnte. Außerdem wurden bei vier von 10 Patienten, bei denen die Lungenembolie in beiden Pulmonalarterien sich befand, alle acht Areale im CT als minderperfundiert definiert, während in Iodkarten des DECT und in SENCEFUL MRT perfundierte Areale interpretiert worden sind. Die Oktanten, welche aufgrund der Lokalisation der Lungenembolie als Areal

mit erwarteter Durchblutungsstörung im CT definiert wurden, hätten, bei einem nicht vollständigen Gefäßverschluss, durchblutet sein können. Ein weiterer wichtiger Aspekt ist die Tatsache, dass das CT in der Peripherie an Sensitivität verliert und kleine Lungenembolien übersehen werden könnten. Dies könnte die Sensitivität und Spezifizität der funktionellen Bildgebungstechniken ebenfalls beeinflusst haben.

Trotz dessen sollte hervorgehoben werden, dass die MRT Methode weder Strahlenbelastung noch eine Applikation eines Kontrastmittels mit dessen einhergehenden Nebenwirkungen impliziert. Da heutzutage die Lungenembolie zunehmend mittels CT diagnostiziert wird, ist der Aspekt der Strahlenbelastung nicht zu vernachlässigen. Ein weiterer Vorteil der SENCEFUL Technik ist die Durchführung in freier Atmung.

Zusammenfassend konnte in dieser Arbeit festgestellt werden, dass die Iodkarten des DECTs im Vergleich zum SENCEFUL MRT eine höhere Sensitivität uns Spezifizität in der Diagnose einer Lungenembolie aufweisen.

9. References

1. Wendelboe AM, Raskob GE. Global Burden of Thrombosis: Epidemiologic Aspects. Circ Res. 2016 Apr 29;118(9):1340–7.

2. Konstantinides SV, Meyer G, Becattini C, Bueno H, Geersing GJ, Harjola VP, et al. 2019 ESC Guidelines for the diagnosis and management of acute pulmonary embolism developed in collaboration with the European Respiratory Society (ERS): The Task Force for the diagnosis and management of acute pulmonary embolism of the European Society of Cardiology (ESC). Eur Heart J. 2020 Jan 21;41(4):543–603.

3. Stein PD, Fowler SE, Goodman LR, Gottschalk A, Hales CA, Hull RD, et al. Multidetector computed tomography for acute pulmonary embolism. N Engl J Med. 2006 Jun 1;354(22):2317–27.

4. Jaschke W, Schmuth M, Trianni A, Bartal G. Radiation-Induced Skin Injuries to Patients: What the Interventional Radiologist Needs to Know. Cardiovasc Intervent Radiol. 2017;40(8):1131–40.

5. Smith-Bindman R. Radiation Dose Associated With Common Computed Tomography Examinations and the Associated Lifetime Attributable Risk of Cancer. Arch Intern Med. 2009 Dec 14;169(22):2078.

6. Diederich S, Lenzen H. Radiation exposure associated with imaging of the chest. Cancer. 2000;89(S11):2457–60.

7. Petritsch B, Kosmala A, Gassenmaier T, Weng AM, Veldhoen S, Kunz AS, et al. Diagnosis of Pulmonary Artery Embolism: Comparison of Single-Source CT and 3rd Generation Dual-Source CT using a Dual-Energy Protocol Regarding Image Quality and Radiation Dose. RöFo - Fortschritte Auf Dem Geb Röntgenstrahlen Bildgeb Verfahr. 2017 Jun;189(6):527–36.

8. Fink C, Johnson TR, Michaely HJ, Morhard D, Becker C, Reiser M, et al. Dual-energy CT angiography of the lung in patients with suspected pulmonary embolism: initial results. ROFO Fortschr Geb Rontgenstr Nuklearmed. 2008 Oct;180(10):879–83.

9. Kunz AS, Weng AM, Wech T, Knapp J, Petritsch B, Hebestreit H, et al. Non-contrast pulmonary perfusion MRI in patients with cystic fibrosis. Eur J Radiol [Internet]. 2021 Jun 1 [cited 2021 Nov 21];139. Available from: https://www.ejradiology.com/article/S0720-048X(21)00133-9/fulltext

10. Fischer A, Weick S, Ritter CO, Beer M, Wirth C, Hebestreit H, et al. SElf-gated Non-Contrast-Enhanced FUnctional Lung imaging (SENCEFUL) using a quasi-random fast low-angle shot (FLASH) sequence and proton MRI. NMR Biomed. 2014 Aug;27(8):907–17.

11. Schumacher G-H, Aumüller G. Topographische Anatomie des Menschen. 7. Auflage. Elsevier, Urban & Fischer; 2004. 460 p.

12. Chaudhry R, Bordoni B. Anatomy, Thorax, Lungs. In: StatPearls [Internet]. Treasure Island (FL): StatPearls Publishing; 2020 [cited 2020 Apr 2]. Available from: http://www.ncbi.nlm.nih.gov/books/NBK470197/

13. Khan YS, Lynch DT. Histology, Lung [Internet]. Treasure Island (FL): StatPearls Publishing; 2020 [cited 2020 Oct 31]. Available from: https://www.ncbi.nlm.nih.gov/books/NBK534789/

14. Schönbach C. Respiratory Tract, Upper and Lower. In: Dubitzky W, Wolkenhauer O, Cho KH, Yokota H, editors. Encyclopedia of Systems Biology [Internet]. New York, NY: Springer; 2013 [cited 2020 Oct 30]. p. 1851–2. Available from: https://doi.org/10.1007/978-1-4419-9863-7_748

15. Bronchial Anatomy: Overview, Gross Anatomy, Microscopic Anatomy [Internet]. [cited 2020 Oct 30]. Available from: https://reference.medscape.com/article/1898852-overview#showall

16. Haddad M, Sharma S. Physiology, Lung [Internet]. In: StatPearls [Internet]. Treasure Island (FL): StatPearls Publishing; 2020 [cited 2020 Oct 31]. Available from: https://www.ncbi.nlm.nih.gov/books/NBK545177/

17. Schünke M, Schulte E, Schumacher U. PROMETHEUS: Texto Y Atlas De Anatomia. Organos Internos / Text and Anatomy Atlas. Internal Organs. Editorial Médica Panamericana S.A.; 2010. 473 p.

18. Kandathil A, Chamarthy M. Pulmonary vascular anatomy & anatomical variants. Cardiovasc Diagn Ther. 2018 Jun;8(3):201–7.

19. Almeida J, Leal C, Figueiredo L. Evaluation of the bronchial arteries: normal findings, hypertrophy and embolization in patients with hemoptysis. Insights Imaging. 2020 Dec;11(1):70.

20. Keller K, Hobohm L, Ebner M, Kresoja KP, Münzel T, Konstantinides SV, et al. Trends in thrombolytic treatment and outcomes of acute pulmonary embolism in Germany. Eur Heart J. 2020 Jan 21;41(4):522–9.

21. Pollack CV, Schreiber D, Goldhaber SZ, Slattery D, Fanikos J, O'Neil BJ, et al. Clinical Characteristics, Management, and Outcomes of Patients Diagnosed With Acute Pulmonary Embolism in the Emergency Department: Initial Report of EMPEROR (Multicenter Emergency Medicine Pulmonary Embolism in the Real World Registry). J Am Coll Cardiol. 2011 Feb 8;57(6):700–6.

22. Shopp JD, Stewart LK, Emmett TW, Kline JA. Findings From 12-lead Electrocardiography That Predict Circulatory Shock From Pulmonary Embolism: Systematic Review and Meta-analysis. Jones AE, editor. Acad Emerg Med. 2015 Oct;22(10):1127–37.

23. Le Gal G, Righini M, Roy PM, Sanchez O, Aujesky D, Bounameaux H, et al. Prediction of Pulmonary Embolism in the Emergency Department: The Revised Geneva Score. Ann Intern Med. 2006 Feb 7;144(3):165–71.

24. Wells PS. Use of a Clinical Model for Safe Management of Patients with Suspected Pulmonary Embolism. Ann Intern Med. 1998 Dec 15;129(12):997.

25. Thomson KR, Varma DK. Safe use of radiographic contrast media. Australian Prescriber. 2010;33:19–22.

26. Authors/Task Force Members, Konstantinides SV, Torbicki A, Agnelli G, Danchin N, Fitzmaurice D, et al. 2014 ESC Guidelines on the diagnosis and management of acute pulmonary embolism. Eur Heart J. 2014 Nov 14;35(43):3033–80.

27. Beckmann M, Boosz A. Diagnostik und Therapie der Venenthrombose und der Lungenembolie. Geburtshilfe Frauenheilkd. 2011 May;71(05):R36–61.

28. Goel A. Compton effect | Radiology Reference Article | Radiopaedia.org [Internet]. Radiopaedia. [cited 2022 Jun 6]. Available from: https://radiopaedia.org/articles/compton-effect

29. Goel A. Photoelectric effect | Radiology Reference Article | Radiopaedia.org [Internet]. Radiopaedia. [cited 2022 Jun 6]. Available from: https://radiopaedia.org/articles/photoelectric-effect?lang=us

30. Godfrey Hounsfield. In: Wikipedia [Internet]. 2022 [cited 2022 Apr 15]. Available from: https://en.wikipedia.org/w/index.php?title=Godfrey_Hounsfield&oldid=1071781424

31. Kalender WA. Computed Tomography: Fundamentals, System Technology, Image Quality, Applications. 3rd revised edition. Wiley; 2011.

32. Thieme SF, Johnson TRC, Reiser MF, Nikolaou K. Dual-Energy Lung Perfusion Computed Tomography: A Novel Pulmonary Functional Imaging Method. Semin Ultrasound CT MRI. 2010 Aug 1;31(4):301–8.

33. Coursey CA, Nelson RC, Boll DT, Paulson EK, Ho LM, Neville AM, et al. Dual-Energy Multidetector CT: How Does It Work, What Can It Tell Us, and When Can We Use It in Abdominopelvic Imaging? RadioGraphics. 2010 Jul 1;30(4):1037–55.

34. Johnson TRC. Dual-Energy CT: General Principles. Am J Roentgenol. 2012 Nov;199(5_supplement):S3–8.

35. Kang MJ, Park CM, Lee CH, Goo JM, Lee HJ. Dual-Energy CT: Clinical Applications in Various Pulmonary Diseases. RadioGraphics. 2010 May;30(3):685–98.

36. Thieme SF, Johnson TRC, Lee C, McWilliams J, Becker CR, Reiser MF, et al. Dual-Energy CT for the Assessment of Contrast Material Distribution in the Pulmonary Parenchyma. Am J Roentgenol. 2009 Jul;193(1):144–9.

37. Pooley RA. AAPM/RSNA physics tutorial for residents: fundamental physics of MR imaging. Radiogr Rev Publ Radiol Soc N Am Inc. 2005 Aug;25(4):1087–99.

38. Currie S, Hoggard N, Craven IJ, Hadjivassiliou M, Wilkinson ID. Understanding MRI: basic MR physics for physicians. Postgrad Med J. 2013 Apr 1;89(1050):209–23.

39. Price RR. The AAPM/RSNA physics tutorial for residents. Contrast mechanisms in gradient-echo imaging and an introduction to fast imaging. RadioGraphics. 1995 Jan 1;15(1):165–78.

40. Thomsen HS, Morcos SK, Almén T, Bellin MF, Bertolotto M, Bongartz G, et al. Nephrogenic systemic fibrosis and gadolinium-based contrast media: updated ESUR Contrast Medium Safety Committee guidelines. Eur Radiol. 2013 Feb;23(2):307–18.

41. Hatabu H, Tadamura E, Levin DL, Chen Q, Li W, Kim D, et al. Quantitative assessment of pulmonary perfusion with dynamic contrast-enhanced MRI. Magn Reson Med. 1999;42(6):1033–8.

42. Mai VM, Berr SS. MR perfusion imaging of pulmonary parenchyma using pulsed arterial spin labeling techniques: FAIRER and FAIR. J Magn Reson Imaging. 1999;9(3):483–7.

43. Bauman G, Puderbach M, Deimling M, Jellus V, Chefd'hotel C, Dinkel J, et al. Non-contrast-enhanced perfusion and ventilation assessment of the human lung by means of fourier decomposition in proton MRI. Magn Reson Med. 2009;62(3):656–64.

44. Stein PD, Chenevert TL, Fowler SE, Goodman LR, Gottschalk A, Hales CA, et al. Gadolinium-enhanced magnetic resonance angiography for pulmonary embolism: a multicenter prospective study (PIOPED III). Ann Intern Med. 2010 Apr 6;152(7):434–43, W142-143.

45. Zhang LJ, Zhao YE, Wu SY, Yeh BM, Zhou CS, Hu XB, et al. Pulmonary Embolism Detection with Dual-Energy CT: Experimental Study of Dual-Source CT in Rabbits. Radiology. 2009 Jul 1;252(1):61–70.

46. Revel MP, Sanchez O, Couchon S, Planquette B, Hernigou A, Niarra R, et al. Diagnostic accuracy of magnetic resonance imaging for an acute pulmonary embolism: results of the 'IRM-EP' study. J Thromb Haemost JTH. 2012 May;10(5):743–50.

47. Bauman G, Puderbach M, Heimann T, Kopp-Schneider A, Fritzsching E, Mall MA, et al. Validation of Fourier decomposition MRI with dynamic contrast-enhanced MRI using visual and automated scoring of pulmonary perfusion in young cystic fibrosis patients. Eur J Radiol. 2013 Dec 1;82(12):2371–7.

10. Appendix

I List of abbreviations

ASL-MRI – Arterial Spin Labeling MRI
B0 – external magnetic field
CI – confidence interval
CT – computed tomography
CTPA – computed tomography pulmonary angiogram
DC – direct current
DCE-MRI – Dynamic Contrast-Enhanced MRI
DECT – Dual-Energy CT
DSCT – Dual-Source CT
DVT – deep vein thrombosis
ECG – electrocardiogram
ESC – European Society of Cardiology
FD – Fourier decomposition
FLASH – fast low angle shot
Gx – frequency encoding gradient or readout gradient
Gy – phase encoding gradient
Gz – slice selection gradient
HU – Hounsfield units
keV – kiloelectron volt
kVp – kilovoltage peak
MRI – Magnetic Resonance Imaging
mSv – millisievert
PE – pulmonary artery embolism/pulmonary embolism
PIOPED – Prospective Investigation of Pulmonary Embolism
RF – radiofrequency
SENCEFUL – Self-gated Non-Contrast-Enhanced FUnctional Lung
SSCT – Single-Source CT
TE – echo time
TR – repetition time

II List of figures

Figure 1: The lung: 1 – superior right lobe; 2 – middle right lobe; 3 – inferior right lobe; 4 – superior left lobe; 5 – inferior left lobe; a – horizontal fissure right; b – oblique fissure right; c – oblique fissure left.

Figure 2: A schematic representation of the bronchial tree, following reference (17).

Figure 3: Diagnostic algorithm of PE. PE: pulmonary embolism; TTE: transthoracic echocardiogram; RV dysfunction: right ventricular dysfunction; CTPA: computed tomography pulmonary angiogram, following reference (2).

Figure 4: A: photoelectric effect; B: Compton scattering. 1: ejected photoelectron; 2: electron of an outer K-shell fills the gap; 3: ejected photoelectron. The representation follows reference (28, 29).

Figure 5: Application of a radiofrequency with the subsequent rotation of the net magnetization to the transverse plane (M: net magnetization; RF: radiofrequency), following reference (37).

Figure 6: Illustration of the magnetic field gradient strength, with slice selection (blue bars-slice location with a specific magnetic field strength), following reference (38).

Figure 7: readout gradient (Gx) and phase encoding gradient (Gy), following reference (38).

Figure 8: FLASH (fast low angle shot) sequence, following reference (39).

Figure 9: SENCEFUL MRI; a = right superior area, b = right inferior area, c = left superior area, d = left inferior area.

Figure 10: Sagittal view of the right lung half, whereby numbers (1–6) indicate the MRI slices; a = right superior frontal area, b = right inferior frontal area, c = right superior dorsal area, d = right inferior dorsal area. The line that divides the superior from the inferior areas is included in the exemplary images of slices 1 and 5.

Figure 11: A: CT scan with PE in segmental artery lingula level; B and C: perfusion maps of DECT slices with visible defect of perfusion in transversal (B) and coronal (C) orientation.

Figure 12: CT slices (a and b) vs. SENCEFUL MRI (c and d). Localization of the embolism highlighted with white arrows.

Figure 13: Four slices of SENCEFUL MR (first row) vs. four corresponding slices of iodine maps of DECT (second row) of the same patient; left to right = frontal to dorsal. The maps show a perfusion impairment mainly in the right lung half, in particular the right superior lobe.

Figure 14: a and b: SENCEFUL MR Images; c and d: corresponding iodine perfusion maps DECT. The maps of SENCEFUL MRI and iodine maps of DECT show a perfusion impairment in the right superior/middle lobe, as well as in the left superior lobe in the frontal layers (highlighted by white arrows). The extent of the perfusion impairments, shown in blue in SENCEFUL MRI and in black in the iodine maps of DECT, have not the same size.

Figure 15: SENCEFUL MRI, two subsequent dorsal slices, a: predominantly perfused, b: complete lack of perfusion.

III List of tables

Table 1: Revised Geneva score. PE: pulmonary embolism; DVT: deep vein thrombosis.

Table 2: Wells score.

Table 3: CTPA vs. iodine maps of DECT; 0 = no thromboembolic material in CTPA/regular perfusion in DECT iodine maps; 1 = thromboembolic material in CTPA/impaired perfusion in DECT iodine maps.

Table 4: CTPA vs. SENCEFUL MR techniques, 0 = no thromboembolic material in CTPA/regular perfusion in SENCEFUL MRI; 1 = thromboembolic material in CTPA/impaired perfusion in SENCEFUL MRI.

IV Acknowledgments

I would like to thank the Institute of Diagnostic and Interventional Radiology of the University of Würzburg and Prof. Dr. med. Simon Veldhoen for letting me work on this study.
A special thank you goes to Dr. Andreas Weng for the help and guidance he gave me during the study. My gratitude also goes to the committee of this doctoral thesis, Prof. Dr. Matthias Eyrich and Prof. Dr. Herbert Köstler.

Thank you to my family, especially to my parents for the loving and caring education they gave me. And to my partner during this chapter of my life, Philipp Eirich, thank you for always having an open ear to listen, and for being patient and supportive.